Static Delay Variation Models for Ripple-Carry and Borrow-Save Adders

Kleanthis Papachatzopoulos, *Student Member, IEEE*, and Vassilis Paliouras, *Member, IEEE*

***Abstract*— This paper introduces two statistical delay-variability models for certain hardware adder implementations, namely, the ripple-carry adder (RCA) and the borrow-save adder (BSA). The introduced models take into account correlated variation sources. Initially, we derive a first proposed model, namely, Type-I model, in the form of expressions for the computation of the exact probability density functions (pdfs) of maximum output delays for Gaussian and non-Gaussian variation sources. Furthermore, we present closed formulas for the covariances between output delays of the aforementioned adder architectures. The introduced derived covariances are subsequently combined with Clark's method to derive a second proposed model, Type-II model, which comprises approximations of the maximum delay pdfs for an RCA and a BSA. Simulation results and the derived exact Type-I PDFs are found to perfectly agree, while the proposed Clark-based Type-II models present an error for standard deviation of maximum delay that increases as BSA word length increases. Both the introduced models and the simulations prove that BSAs achieve narrower delay distributions than RCAs, i.e., they significantly reduce delay variance. Consequently, BSAs are proven to be suitable for variation-tolerant applications by providing a timing safety margin, when compared to RCA architectures. The underlying analysis indicates that for the case of BSA and either intra-die delay variations only or both intra- and inter-die delay variations, the Type-II models introduce non-negligible errors, which are as much as 16% of the standard deviation of maximum delay for a 256-digit BSA, as the Type-II Gaussian pdf approximations deviate significantly from the exact Type-I PDFs. However, for all RCA and BSA inter-die only variation cases, both types present satisfactory accuracy due to the Gaussian shape of exact pdfs.**

***Index Terms*— Adder variability, borrow-save encoding, high-radix adder, ripple-carry adder, statistical timing analysis, variation-tolerant design.**

I. Introduction

DEEP Sub-micron Era in VLSI design has arrived and a cost imposed is the adoption of design methodologies that enhance the noise immunity of contemporary ICs. Noise margins are drastically exacerbated by the combination of low supply voltages and shrinking device dimensions increasing variability in several device characteristics. Process variability is attributed to the gap between manufacturing tolerances and technology scaling [1]–[3]. The device parameters of bulk CMOS technology affected mostly are the threshold voltage, V_{th}, transistor/interconnection length and width, and oxide thickness, which impact to a great extend both on timing and power yield. Indicative of variability effects is the fact that, moving from the 130-nm to the 45-nm technology node, standard deviation of threshold voltage almost doubled, while its nominal value inclined from almost 350 mV to 280 mV [4].

It is common in the literature that the device parameter variations are separated into *intra-die* and *inter-die* components for modeling purposes. *Inter-die* variability is due to mechanisms that induce *systematic variations* across a wafer, lot, or die, acting in a systematic and predictable way, and affect globally the respective device parameters [2], [3]. On the contrary, *intra-die* variations for planar bulk CMOS technologies are caused by *random fluctuations* and Line-Edge Roughness (LER), and/or *atomic-level differences* of device parameters, such as the number and placement of dopant atoms in MOSFETs [1]–[3], [5], [6]. It is known that the effect of inter-die variations prevails over that of intra-die variations as the logic depth increases [2]. Nonetheless, the contribution of the latter seems to dominate in contemporary technology nodes with low supply voltages, in which the logic depth is significantly reduced in order to maximize frequency [5]. We employ a linear delay model in order to capture fluctuations on delays, as the linearity assumption for the delay variation modeling is common in [7].

We mainly focus on the delay variations caused by the aforementioned mechanisms on hardware implementations of certain adder architectures. In the presence of variations, hardware architectures that exploit certain encoding schemes have been proven more efficient, under specific criteria, than conventional binary arithmetic. In [8], it is shown that multiply-accumulate units based on Residue Number System (RNS) representation present better normalized delay characteristics than the binary structures with the same dynamic range. Recently, adopting CMOS BSIM 4 models, an analysis by Papachatzopoulos and Paliouras [9] has revealed that not only does borrow-save encoding lead to hardware implementations that have substantially smaller standard deviation of maximum delay than RCAs, but they also demonstrate significant power dissipation benefits. Further prior work addresses the impact of process and environmental fluctuations on delay variations. Bernstein *et al.* [10] present a variability analysis for selected 16-bit adder topologies, quantifying the normalized delay variability for each adder architecture in Static and Dynamic styles, and showing that V_{th} variability is the primary contributor to delay variability. Alioto and Palumbo [11] provide

Manuscript received October 3, 2018; revised January 9, 2019; accepted February 12, 2019. Date of publication March 12, 2019; date of current version June 18, 2019. This paper was recommended by Associate Editor X. Zhang. *(Corresponding author: Kleanthis Papachatzopoulos.)*

The authors are with the Department of Electrical and Computer Engineering, School of Engineering, University of Patras, 26504 Patras, Greece (e-mail: papachatz@ece.upatras.gr; paliuras@ece.upatras.gr).

Color versions of one or more of the figures in this paper are available online at http://ieeexplore.ieee.org.

Digital Object Identifier 10.1109/TCSI.2019.2900151

analytical models that allow an understanding of voltage sensitivity of Mirror and Dual-Rail Full Adders, resorting to simplified circuit models. Alioto *et al.* [12] propose a framework for the estimation of max-delay variability of circuit paths that relies on the FO4 metric and on a cell-specific coefficient, which is independent of PVT conditions and technology generations. Eisele *et al.* [5] demonstrate the increased normalized path delay variation of a Carry-Select Adder due to local V_{th} variations. Abu-Rahma and Anis [13] develop a model for a CMOS inverter that links the variance of V_{th} and propagation delay, proving that they are proportional and dependent on the value of supply voltage.

Contributions: This manuscript focuses on the derivation and evaluation of two types of statistical delay-variability models for RCAs and BSAs. Specifically,

1) Formulas for the exact Probability Density Function (PDF) of the maximum output delay for the Ripple-Carry Adder (RCA) and the Borrow-Save Adder (BSA) in the presence of delay variations are derived. In the following, we refer to these models as Type-I models;
2) Closed formulas are derived, given as *Lemmas* 1, 2, and 3, that compute the covariances between the output delays of an adder structure, either RCA or BSA;
3) Subsequently, the derived covariances are utilized to approximate the maximum delay distribution for each of the two architectures. The approximation relies on Clark's expressions [14], and it is assumed that the delay is modeled statically, *i.e.*, without applying any vectors at the input of the respective circuits. We refer to this model as Type-II model;
4) The agreement of the proposed models with simulation data is investigated: Furthermore using both models, it is proven statistically that BSAs outperform RCAs in the presence of delay variations. In addition, as Monte-Carlo simulations of long bit-length implementations are generally prohibitive due to excessive simulation time, our models contribute to fast delay modeling for the particular adder implementations. In this context, statistical delay metrics of 4- to 256-digit BSA implementations are demonstrated and discussed.

Although less accurate than the proposed Type-I model, the Clark-based Type-II model finds applicability in *Statistical Static Timing Algorithms* that demand the same delay representation in all nodes of the examined circuit, referred as canonical delay models [2], [7].

The remainder of this paper is structured as follows: In Section II, a review of the Ripple-Carry Adder and High-Radix Adder with borrow-save encoding is provided. Section III introduces the proposed Type-I models for RCAs and BSAs. In Section IV, the correlation coefficients between output delays in RCAs and in BSAs are derived and utilized to construct the proposed Type-II models for the two aforementioned adders. An extension of the derived models for the Carry-Select Adder is presented in Section V. In Section VI, a comparison of RCA and BSA based on statistical metrics of the proposed models takes place, and the agreement with the experimental data is investigated. Finally, Section VII presents conclusions.

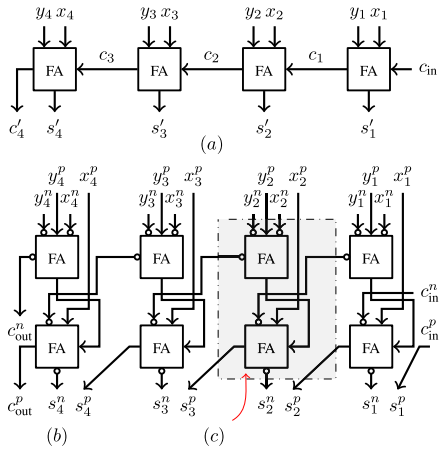

Fig. 1. Architecture of *a*) 4-bit Ripple-Carry Adder, *b*) Radix-16 Adder with borrow-save encoding, and *c*) 4-to-2 compressor implemented by two Full Adders (gray-shaded area).

II. Ripple-Carry Adder and High-Radix Adder With Borrow-Save Encoding

Ripple-Carry Adders are common for adding numbers expressed in conventional binary arithmetic. They consist of Full-Adder (FA) cells connected sequentially with the carry-out output of an FA driving the carry-in input of the subsequent one. More often than not, the delay of an FA from carry-in to carry-out path is optimized so the critical path delay along a carry chain, formed by cascaded FAs, is minimized [15]. This linear-to-the-word-length delay dependence compromises the maximum operation frequency for long bit-length RCAs. Therefore, alternative adder architectures have been proposed, such as Carry-Skip, Carry-Select and Kogge-Stone Adders [16]. However, RCAs are used as a building block for a range of hybrid adder architectures [15], [16]. In parallel, the area of an N-bit RCA, A_{RCA}, is $A_{\text{RCA}} \approx N \cdot A_{\text{FA}}$, where A_{FA} is the area of a FA.

High-Radix architectures add digits encoded in a radix-r number system that assume values in the set $[0, r-1]$, where r is an integer. In order to speed up addition, a redundant radix-r digit set can be employed, which allows the existence of redundant representations. A radix-r digit set must comprise more that r digit values in order to be redundant. One such representation, called radix-2 or borrow-save encoding, uses digits in the set $S \in \{-1, 0, 1\}$, where each digit value, x, can be expressed as the sum of a bit with positive, x^p, and a bit with negative weight, x^n, as $x = x^p - x^n$. As an example, 0 has two different representations as (x^p, x^n)=(0, 0)=0+0=0 and $(x^p, x^n) = (1, 1)$=1−1=0.

A number of different architectures for the (multi-operand) addition operation have been proposed which adopt redundant representations [17]. Among them, particularly interesting is the one in [18], in which a pair of digits expressed in borrow-save encoding is added using a 4-to-2 compressor, which consists of two FA cells. An N-digit BSA implements the *carry-free addition algorithm* [16] and occupies an area A_{BSA}, with $A_{\text{BSA}} \approx 2N \cdot A_{\text{FA}}$. The structure of a radix-16 adder of the aforementioned architecture, as assumed in the remainder of the manuscript, is displayed in Fig. 1(b), while Fig. 1(c)

depicts two FAs connected to form a 4-to-2 compressor (slice). The critical path of a BSA incorporates only two FA cells and is independent of the word length of the operands.

III. Type-I Maximum Delay PDFs for RCA and BSA

This section presents expressions for the Probability Density Functions of maximum delays for the Ripple-Carry Adder and the Borrow-Save Adder in the presence of delay variations. The presented statistical models consider the correlation between the delays of constituent adder components. Before the derivation of RCA and BSA PDFs, we describe the corresponding delay models and define the related notation.

A. Assumptions Employed by the Proposed Models

In the context of timing analysis, delay variability is treated using Random Variables (RVs), motivated by the recent advances in *Statistical Timing Analysis* [2], [3] that model delay variations as RVs with specific PDF. Additionally, the fact that the variance of the propagation delay of a cell is proportional to the variance of V_{th} [13] allows modeling the total delay of cells as RVs effectively hiding technology-dependent parameters.

In our analysis, a set of dependent RVs models adder output delays. The derivation of the proposed Type-I model relies on two transformations in order to construct the joint PDF of dependent RVs exploiting known PDFs of correlated primitive cell delay RVs and the circuit architecture. For all derivations, a static delay model is employed. Additionally, it is assumed that the mean delay values of primary outputs correspond to the mean values of maximum delay paths that end to the particular output. The corresponding mean values of each output are obtained by traversing the circuit graphs in a depth-first manner.

In this work, viability analysis is not considered as a pre-processing step for the computation of maximum delay PDFs. In case they exist, such paths are removed beforehand. The models compute the exact maximum delay PDFs described by closed-form expressions and taking into account the delays of all paths, in contrast to other works (cf. [19]) which propose path-based techniques and compute a set of viable paths with the greatest delay distributions.

We focus on FA implementations of practical interest in terms of area and Power-Delay Product [20], and we make related abstractions in order our models to reflect the respective adder structures. In more detail, in this paper we focus on FA cells that produce the sum output in parallel with the carry output, as in case of CPL, Transmission Gate, and Dual-Rail Domino Full Adders [11], [20], [21]. A thorough analysis for performance and Power-Delay Product benefits of CPL can be found in [22]. Use of a different FA architecture would require appropriate modification of the presented models.

We assume that the delay of an N-bit RCA at the jth sum output, s'_j, for $j = 1, 2, \ldots, N$ is linearly dependent on the delays of the cells comprising the path from inputs to the jth sum output, and is given by

$$s'_j = s_j + \sum_{k=1}^{j-1} c_k, \tag{1}$$

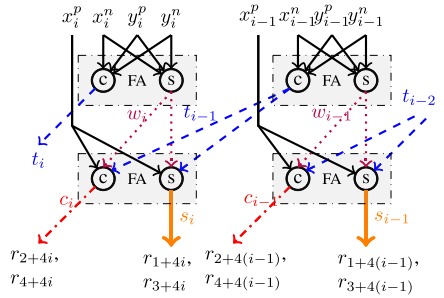

Fig. 2. Paths of a Borrow-Save Adder with separate generation of carry and sum outputs for each Full Adder. Dotted and bolt edges constitute path delay r_{1+4i}, dotted and dash-dotted edges constitute r_{2+4i}, dashed and bolt edges constitute r_{3+4i}, and dashed and dash-dotted edges constitute r_{4+4i} of ith compressor. Inverters are omitted.

where c_k models carry generation/propagation delay at FA k, and s_j represents the sum delay at FA j. The delay at the jth carry output, determined by the carry-chain delay, is

$$c'_j = \sum_{k=1}^{j} c_k. \tag{2}$$

The proposed Type-I models as well as the derived covariance relations are independent of the nature of variation mechanism. However, for the experiments in Section VI we assume Gaussian variations (cf. [2], [3]).

Sum delay s_i, as well as any other delay, is decomposed as

$$s_i = s_{i,\text{nom}} + s_{i,\text{var}}, \tag{3}$$

where $s_{i,\text{nom}}$ constitutes the nominal value of s_i, which is a deterministic value, and $s_{i,\text{var}}$ is the respective variation. In case of intra-die and inter-die variations, *i.e.*, completely independent or dependent variations between sub-unit delays, $s_{i,\text{intra}}$ and $s_{i,\text{inter}}$ notation is used for the random component of the delay, respectively. When $s_{i,\text{intra}}$ and $s_{i,\text{inter}}$ are independently distributed zero-mean RVs, sum delay s_i is also a RV with mean value $\mu_{s_i} = s_{i,\text{nom}}$ and variance $\sigma^2_{s_i} = \sigma^2_{s_{i,\text{intra}}} + \sigma^2_{s_{i,\text{inter}}}$.

As far as the notation for BSA architecture is considered, RV w_i describes the sum delay of the ith upper-row FA, and t_{i-1} the carry delay of the $(i-1)$st upper-row FA, while s_i and c_i describe the sum and carry delays of the ith lower FA, respectively. The respective cell delays are clarified in Fig. 2. Fan-out and sizing optimization are not taken into account. However, structural similarities in the two adder architectures imply identical dependence on these parameters. In addition, interconnection delay and its relevant variability are not considered. For this reason, RVs s_i and w_i have the same mean, $\mu_{s_i} = \mu_{w_i} = s_{\text{nom}}$, and standard deviation, $\sigma_{s_i} = \sigma_{w_i} = \sigma_s$, as well as c_i and t_{i-1} have the same mean, $\mu_{c_i} = \mu_{t_{i-1}} = c_{\text{nom}}$, and standard deviation, $\sigma_{c_i} = \sigma_{t_{i-1}} = \sigma_c$. It is noted that delay components of w_i are independently distributed, thus, $\sigma^2_{w_i} = \sigma^2_{w_{i,\text{intra}}} + \sigma^2_{w_{i,\text{inter}}}$. The same assumption holds also for the RVs t_{i-1}, s_i, and c_i.

B. CDF of Maximum of Ripple-Carry Adder Path Delays

1) General Case for RCA: The following derivation refers to delay variations that affect the delay of an N-bit RCA,

for correlation coefficients among primitive cell delays less than one. The case where variations are completely dependent is presented in Section III-B.2. Correlations among paths are captured through a linear transformation.

The Cumulative Density Function (CDF) of RV $Z = \max\{S'_1, S'_2, \ldots, S'_N, C'_N\}$ is readily obtained from the joint CDF of $\mathbf{S}^* = [S'_1, S'_2, \ldots, S'_N, C'_N]^T$. Since Z is the maximum of $S'_1, S'_2, \ldots, S'_N, C'_N$,

$$\begin{aligned}\mathrm{cdf}(Z) &= \mathrm{P}(z \le Z) \quad (4)\\ &= \mathrm{P}(s'_1 \le Z \wedge s'_2 \le Z \wedge \cdots \wedge s'_N \le Z \wedge c'_N \le Z)\\ &= \mathrm{cdf}_{\mathbf{S}^*}(Z, Z, \ldots, Z). \quad (5)\end{aligned}$$

Due to the circuit structure, S'_i, $i = 1, 2, \ldots, N$, and C'_N are dependent RVs. To derive their joint PDF, we express output RVs as linear combinations of primary cell delay RVs as

$$S'_i = C_1 + C_2 + \ldots + C_{i-1} + S_i, \quad (6)$$

$$C'_i = C_1 + C_2 + \ldots + C_{i-1} + C_i, \quad (7)$$

exploiting the circuit structure according to (1) and (2). We introduce $N-1$ dummy variables U_j, for $j = 1, 2, \ldots, N-1$, to achieve a square transformation matrix, and generalizing (6) and (7), the following transformation is obtained

$$\mathbf{S}' = \begin{bmatrix} \mathbf{I}_N & \mathbf{A}_N \\ \mathbf{0}_N & \mathbf{B}_N \end{bmatrix} \cdot \mathbf{S}, \quad (8)$$

where

$$\begin{aligned}\mathbf{S}' &= \begin{bmatrix} S'_1 & S'_2 & \cdots & S'_N & C'_N & U_1 & U_2 & \cdots & U_{N-1} \end{bmatrix}^T,\\ \mathbf{S} &= \begin{bmatrix} S_1 & S_2 & \cdots & S_N & C_1 & C_2 & \cdots & C_N \end{bmatrix}^T, \quad (9)\end{aligned}$$

$\mathbf{I}_k$ is the $k \times k$ identity matrix, $\mathbf{0}_k$ is a $k \times k$ zero matrix, and matrices $\mathbf{A}_N$ and $\mathbf{B}_N$ have elements

$$A(k,l) = \begin{cases} 1, & \text{if } k > l, \\ 0, & \text{otherwise}, \end{cases} \quad (10)$$

$$B(k,l) = \begin{cases} 1, & \text{if } k = l \text{ or } k = 1, \\ 0, & \text{otherwise}. \end{cases} \quad (11)$$

The transformation matrix is invertible as it is upper triangular by construction, and the inverse form of (8) is

$$\mathbf{S} = \begin{bmatrix} \mathbf{I}_N & \mathbf{C}_N \\ \mathbf{0}_N & \mathbf{D}_N \end{bmatrix} \cdot \mathbf{S}', \quad (12)$$

where matrices $\mathbf{C}_N$ and $\mathbf{D}_N$ have elements

$$C(k,l) = \begin{cases} -1, & \text{if } l = 1 \text{ and } k > 1, \\ 1, & \text{if } l \ge k \text{ and } k > 1, \\ 0, & \text{otherwise}. \end{cases} \quad (13)$$

$$D(k,l) = \begin{cases} 1, & \text{if } k = l, \\ -1, & \text{if } k = 1 \text{ and } l > 1, \\ 0, & \text{otherwise}. \end{cases} \quad (14)$$

The inverse transformation matrix is derived in Appendix A.

Since the obtained transformation matrix is upper triangular, the Jacobian, J, of the transformation is the product of its diagonal elements [23], which is 1 in our case. As an example, for the 3-bit case, the joint PDF of $S'_1, S'_2, S'_3, C'_3, U_1, U_2$, is

$$\begin{aligned}&\mathrm{pdf}_{S'_1,S'_2,S'_3,C'_3,U_1,U_2}(s'_1, s'_2, s'_3, c'_3, u_1, u_2)\\ &\quad = |J|\,\mathrm{pdf}_{S_1,S_2,S_3,C_1,C_2,C_3}(s'_1, s'_2 - c'_3 + u_1 + u_2,\\ &\qquad s'_3 - c'_3 + u_2, c'_3 - u_1 - u_2, u_1, u_2). \quad (15)\end{aligned}$$

In the extreme case of intra-die variations, exploiting the independence between S_i and C_i, as well as the structure of the transformation matrix, (15) is generalized to

$$\begin{aligned}&\mathrm{pdf}_{\mathbf{S}'}(s'_1, s'_2, \ldots, s'_N, c'_N, u_1, u_2, \ldots, u_{N-1})\\ &\quad = \mathrm{pdf}_{S_1}(s'_1) \prod_{i=2}^{N} \mathrm{pdf}_{S_i}(s'_i - c'_N + \sum_{k=1}^{N-i} u_{N-k})\\ &\qquad \cdot \mathrm{pdf}_{C_1}(c'_N - \sum_{k=1}^{N-1} u_k) \prod_{i=2}^{N-2} \mathrm{pdf}_{C_i}(u_{i-1}). \quad (16)\end{aligned}$$

We derive the joint PDF of $S'_1, S'_2, \ldots, S'_N, C'_N$ by computing a marginal joint PDF that eliminates the dummy variables by integrating over their domain, as

$$\begin{aligned}&\mathrm{pdf}_{\mathbf{S}^*}(s'_1, s'_2, \ldots, s'_N, c'_N)\\ &\quad = \int_{u_1}\int_{u_2}\cdots\int_{u_{N-1}} \mathrm{pdf}_{\mathbf{S}'}(s'_1, s'_2, \ldots, s'_N, c'_N,\\ &\qquad u_1, u_2, \ldots, u_{N-1}) du_{N-1} \ldots du_2 du_1. \quad (17)\end{aligned}$$

Using (17), we derive the CDF of $Z = \max\{\max_{i=1,2,\ldots,N}\{S'_i\}, C'_N\}$, as

$$\begin{aligned}\mathrm{cdf}(Z) = \int_{-\infty}^{Z}\int_{-\infty}^{Z}\cdots\int_{-\infty}^{Z} &\mathrm{pdf}_{\mathbf{S}^*}(s'_1, s'_2, \ldots, s'_N, c'_N)\\ &\times ds'_1 ds'_2 \cdots ds'_N dc'_N. \quad (18)\end{aligned}$$

It is important to note that the derived Type-I model of (15)–(18) is independent of the underlying variation PDFs.

2) Inter-Die Variations Case for RCA: As inter-die random delay variables influence both sum and carry FA delays by the same amount of variations, and in order to simplify notation, RV x_{inter} refers to the inter-die RV component of an FA delay, *i.e.*, $x_{\text{inter}} = s_{k,\text{inter}} = c_{k,\text{inter}}$. Thus, for the case of inter-die delay variations, the CDF of maximum of RCA output delays is written as

$$\begin{aligned}\mathrm{cdf}(Z) &= P(s'_1 < Z, s'_2 < Z, \ldots, s'_N < Z, c'_N < Z)\\ &= P(\mu_s + x_{\text{inter}} < Z, \mu_s + \mu_c + 2x_{\text{inter}} < Z, \ldots,\\ &\quad (n-1)\mu_c + \mu_s + nx_{\text{inter}} < Z, n\mu_c + nx_{\text{inter}} < Z)\\ &= P(\max\{(n-1)\mu_c + \mu_s, n\mu_c\} + nx_{\text{inter}} < Z), \quad (19)\end{aligned}$$

as practical values of $\mu_c, \mu_s, x_{\text{inter}}$, lead to positive delays.

In contrast with the generic PDF of (16), the PDF for the maximum of path delays for inter-die variations observes the same distribution as that of delay variations. Assuming Gaussian variations, the maximum delay PDF under inter-die variations follows the same distribution as that of RV x_{inter}, with a shift of its mean value.

3) Combined Inter-Die and Intra-Die Variations Case for RCA: Assuming that the manifested intra-die and inter-die delay variations are independent, then the maximum delay PDF under both types of delay variations is derived as the convolution of individual PDFs [2] as

$$\mathrm{pdf}_{\mathrm{inter,\,intra}}(Z) = \int_{-\infty}^{+\infty} \mathrm{pdf}_{\mathrm{inter}}(t)\,\mathrm{pdf}_{\mathrm{intra}}(Z-t)dt. \quad (20)$$

C. CDF of Maximum of Borrow-Save Adder Path Delays

1) Case of a Single BSA Slice: As the structure of a BSA is highly regular, we commence the derivation of the CDF of maximum path delays in a BSA by finding the maximum delay of the paths of a single slice. The path delays of the ith slice of a BSA are shown in Fig. 2, and their values are

$$\begin{aligned} r_{1+4i} &= w_i + s_i, \quad r_{2+4i} = w_i + c_i, \\ r_{3+4i} &= t_{i-1} + s_i, \quad r_{4+4i} = t_{i-1} + c_i. \end{aligned} \quad (21)$$

To simplify notation we drop the additive term $4i$ from the subscripts of rs. It can be observed that $r_1 = r_2 + r_3 - r_4$, therefore, a 4×4 matrix describing a transformation from (w, s, t, c) to (r_1, r_2, r_3, r_4) would not be full rank. Defining $\mathbf{A}_{3\times4}$ as

$$\mathbf{A}_{3\times4} = \begin{bmatrix} 1 & 0 & 0 & 1 \\ 0 & 1 & 1 & 0 \\ 0 & 1 & 0 & 1 \end{bmatrix}, \quad (22)$$

the following is a full-rank transformation

$$\begin{bmatrix} r_2 & r_3 & r_4 \end{bmatrix}^T = \mathbf{A}_{3\times4} \cdot \begin{bmatrix} w & t & s & c \end{bmatrix}^T. \quad (23)$$

Given the joint PDF of a set of three out of four path delays per slice, *e.g.*, r_2, r_3, and r_4, the delay of the remainder path, *e.g.*, r_1, has a deterministic value, since $r_1 = r_2 + r_3 - r_4$. Hence, the PDF of r_1 is expressed as

$$\mathrm{pdf}(r_1|r_2, r_3, r_4) = \delta(r_1 - r_2 - r_3 + r_4), \quad (24)$$

and the joint PDF of all four variables r_1, r_2, r_3, r_4, is

$$\begin{aligned} \mathrm{pdf}(r_1, r_2, r_3, r_4) &= \mathrm{pdf}(r_1|r_2, r_3, r_4)\,\mathrm{pdf}(r_2, r_3, r_4) \quad (25) \\ &= \delta(r_1 - r_2 - r_3 + r_4)\,\mathrm{pdf}(r_2, r_3, r_4). \quad (26) \end{aligned}$$

Eq. (26) is used to derive a CDF for a slice as follows

$$\begin{aligned} \mathrm{cdf}(Z) = \int_{-\infty}^{Z}\int_{-\infty}^{Z}\int_{-\infty}^{Z}\int_{-\infty}^{Z} & \delta(r_1 - r_2 - r_3 + r_4) \\ & \cdot \mathrm{pdf}(r_2, r_3, r_4)dr_1dr_2dr_3dr_4. \end{aligned} \quad (27)$$

With a change of variables, (27) is reexpressed as

$$\begin{aligned} \mathrm{cdf}(Z) &= \int_{-\infty}^{Z}\int_{-\infty}^{Z}\int_{-\infty}^{Z}\int_{-\infty}^{Z-r_2-r_3+r_4} \delta(x) \\ &\quad \cdot \mathrm{pdf}(r_2, r_3, r_4)dx dr_2 dr_3 dr_4 \quad (28) \\ &= \underbrace{\int_{-\infty}^{Z}\int_{-\infty}^{Z}\int_{-\infty}^{Z}}_{Z-r_3+r_4\geq r_2} \mathrm{pdf}(r_2, r_3, r_4)dr_2dr_3dr_4. \quad (29) \end{aligned}$$

Eq. (29) assumes that for every value of Z, there always exists a triplet (r_2, r_3, r_4), with $r_2 \leq Z$, $r_3 \leq Z$, $r_4 \leq Z$, such that $Z - r_2 - r_3 + r_4 \geq 0$. Such a solution is obtained if, for example, $r_3 = Z$ and $r_2 < r_4$ for any value of Z.

Taking into account the constraint $Z - r_3 + r_4 > r_2$ of (29) as well as the limits of integrals, $r_2 < Z$, $r_3 < Z$, and $r_4 < Z$, we can distinguish two cases

$$r_2 < Z + r_4 - r_3, \quad \text{and } r_3 < Z, \text{ and } r_4 < r_3, \quad (30)$$

and

$$r_2 < Z, \quad \text{and } r_3 < r_4, \text{ and } r_4 < Z, \quad (31)$$

which lead to the following CDF for a slice of a BSA

$$\begin{aligned} \mathrm{cdf}(Z) &= \mathrm{P}(r_4 < Z, r_4 < r_3 < Z, r_2 < Z - r_3 + r_4) \\ &\quad + \mathrm{P}(r_4 < Z, r_3 < r_4, r_2 < Z) \quad (32) \\ &= \int_{r_4=-\infty}^{Z}\int_{r_3=r_4}^{Z}\int_{r_2=-\infty}^{Z-r_3+r_4} \mathrm{pdf}(r_2, r_3, r_4)dr_2dr_3dr_4 \\ &\quad + \int_{r_4=-\infty}^{Z}\int_{r_3=-\infty}^{r_4}\int_{r_2=-\infty}^{Z} \mathrm{pdf}(r_2, r_3, r_4)dr_2dr_3dr_4. \quad (33) \end{aligned}$$

2) Generalization to the k-Variate Case: Assume an k-digit BSA, which implies that $3k$ paths, r_{2+4i}, r_{3+4i}, r_{4+4i}, $i = 0, 1, \ldots, k-1$ are modeled as RVs and additional k paths are defined in a deterministic way from the $3k$ random paths,

$$r_{1+4i} = r_{2+4i} + r_{3+4i} - r_{4+4i}. \quad (34)$$

For an k-digit BSA, we write

$$[r_1, r_2, \cdots, r_{3k}]^T = (I_k \otimes A_{3\times4}) \cdot [w_1, t_1, \cdots, c_k]^T, \quad (35)$$

where $\otimes$ stands for the Kronecker product. Now we define

$$\mathbf{T}_{3k} = \mathbf{I}_k \otimes \mathbf{A}_{3\times4}. \quad (36)$$

The covariance matrix of *three* paths per slice for an k-digit BSA is then given as

$$\Sigma_{r3} = \mathbf{T}_{3k}\Sigma_w\mathbf{T}_{3k}^T \quad (37)$$

and Σ_w the covariance matrix of cell delays $w_1, t_1, \ldots, s_k, c_k$.

The CDF requires $2k$ integrals with respect to the variables r_{3+4i}, r_{4+4i} each in the interval $(-\infty, Z)$, and k integrals with respect to the variables r_{2+4i} in the interval $(-\infty, Z - r_{3+4i} + r_{4+4i})$.

The CDF of the maximum delay in an k-slice BSA is

$$\begin{aligned} \mathrm{cdf}(Z) = \underbrace{\int_{-\infty}^{Z}\int_{-\infty}^{Z}\cdots\int_{-\infty}^{Z}}_{\substack{Z-r_{2+4i}-r_{3+4i}+r_{4+4i}\geq0, \\ i=0,1,\ldots,k-1}} & \mathrm{pdf}\left(r_2, r_3, r_4, \ldots, r_{2+4(k-1)},\right. \\ & \left. r_{3+4(k-1)}, r_{4+4(k-1)}\right) dr_2dr_3dr_4\ldots \\ & dr_{2+4(k-1)}dr_{3+4(k-1)}dr_{4+4(k-1)}, \end{aligned} \quad (38)$$

where pdf is a multivariate Gaussian obtained using (37).

3) Inter-Die Variations Case for BSA: The delay of a single slice suffices to describe the delay of a BSA, as all slices are subjected to the same delay variations. Assuming that RV x_{inter} represents zero-mean inter-die delay variations, the CDF of BSA is given by

$$\begin{aligned}\text{cdf}(Z) &= P(\mu_w + x_{\text{inter}} + \mu_s + x_{\text{inter}} < Z,\\ &\quad \mu_w + x_{\text{inter}} + \mu_c + x_{\text{inter}} < Z,\\ &\quad \mu_t + x_{\text{inter}} + \mu_s + x_{\text{inter}} < Z,\\ &\quad \mu_t + x_{\text{inter}} + \mu_c + x_{\text{inter}} < Z) \qquad (39)\\ &= P(\max\{\mu_w + \mu_s, \mu_w + \mu_c,\\ &\quad \mu_t + \mu_s, \mu_t + \mu_c\} + 2x_{\text{inter}} < Z). \qquad (40)\end{aligned}$$

Using the transformation $y = 2x_{\text{inter}} + \mu_{\text{inter}}^{\text{BSA}}$, where

$$\mu_{\text{inter}}^{\text{BSA}} = \max\{\mu_w + \mu_s, \mu_w + \mu_c, \mu_t + \mu_s, \mu_t + \mu_c\}, \qquad (41)$$

it holds that $f_Y(y) = \frac{1}{2} f_X(x)$, and (40) is written as

$$\text{cdf}(Z) = \int_{-\infty}^{Z} f_Y(y)dy = \frac{1}{2}\int_{-\infty}^{Z} f_X\left(\frac{y - \mu_{\text{inter}}^{\text{BSA}}}{2}\right)dy, \qquad (42)$$

which means that the maximum is a RV with mean $\mu_{\text{inter}}^{\text{BSA}}$ and standard deviation $2\sigma_{x_{\text{inter}}}$.

D. General PDF Transformation

A transformation described by an invertible full-rank matrix is obtained by introducing to (23) a dummy variable u,

$$\begin{bmatrix} r_2 \\ r_3 \\ r_4 \\ u \end{bmatrix} = \begin{bmatrix} 1 & 0 & 0 & 1 \\ 0 & 1 & 1 & 0 \\ 0 & 1 & 0 & 1 \\ 0 & 0 & 0 & 1 \end{bmatrix} \cdot \begin{bmatrix} w \\ t \\ s \\ c \end{bmatrix} = \mathbf{A} \cdot \begin{bmatrix} w \\ t \\ s \\ c \end{bmatrix}. \qquad (43)$$

Transformation matrix $\mathbf{A}$ is full-rank and invertible, hence

$$[w, t, s, c]^T = \mathbf{A}^{-1} \cdot [r_2, r_3, r_4, u]^T. \qquad (44)$$

Given the joint pdf of w, t, s, c, denoted by $f_{w,t,s,c}$, we use (44) to obtain the joint pdf of r_2, r_3, r_4, as

$$f_{r_2,r_3,r_4}(r_2, r_3, r_4) = \int_u f_{w,t,s,c}(r_2 - u, r_4 - u, r_3 - r_4 + u, u)du, \qquad (45)$$

since the Jacobian of the transformation has $|J| = 1$.

The extension to the k-slice case using the Kronecker product is straightforward. Let

$$\mathbf{r}_u = \left[r_{2i+2}, r_{2i+3}, r_{2i+4}, u_{2i} | i = 0, 1, \ldots, k-1\right]^T, \qquad (46)$$

$$\mathbf{w} = \left[\, w_1,\ w_2,\ \cdots,\ w_{4k} \,\right]^T. \qquad (47)$$

Then

$$\mathbf{r}_u = (I_k \otimes A)\, \mathbf{w} \qquad (48)$$

or

$$\mathbf{w} = \left(I_k \otimes A^{-1}\right) \mathbf{r}_u. \qquad (49)$$

Then the joint pdf of the paths r is given by the marginal pdf over all dummy variables u,

$$\text{pdf}(\mathbf{r}) = \int_{\mathbf{u}} \text{pdf}_{\mathbf{w}}\left(\left(I_k \otimes A^{-1}\right) \mathbf{r}_u\right) d\mathbf{u}, \qquad (50)$$

where $\text{pdf}_{\mathbf{w}}$ is the joint pdf of the primitive delays $\mathbf{w}$, and $\mathbf{r}$ and $\mathbf{u}$ are $3k \times 1$ and $k \times 1$ vectors, defined as

$$\mathbf{r} = \left[r_{2i+2}, r_{2i+3}, r_{2i+4}, | i = 0, 1, \ldots, k-1\right]^T \qquad (51)$$

$$\mathbf{u} = \left[\, u_0,\ u_2,\ \cdots,\ u_{2(k-1)} \,\right]^T. \qquad (52)$$

IV. Correlation Coefficients and Type-II Maximum Delay PDFs for RCA and BSA

This section derives the proposed Type-II models; specifically, they are approximations of maximum delay PDFs of RCA and BSA based on Clark's expressions [14]. Our motivation for using Clark's expression is the simplicity of the technique and the fact that certain *Statistical Static Timing Algorithms* require a unified representation of delay in all nodes of a circuit graph [2]. In more detail, covariances of any two output path delays of a RCA or a BSA are computed taking into account the correlation between primitive delays. The derived results are subsequently used to obtain an approximation of RCA and BSA maximum delay PDFs as Gaussian distributions based on Clark's method.

A. Covariances for RCA Outputs in the Presence of Variations

This subsection refers to the case of an N-bit RCA under delay variations. The delay models follow the definitions given by (1)–(3). The definition of the covariance between RVs k and l is given in [23] as

$$\text{Cov}(k, l) = E[k \cdot l] - E[k] \cdot E[l]. \qquad (53)$$

Specifically, we focus on the computation of covariance between primary output $s_{i'}$ and $s_{j'}$.

Lemma 1: The covariance of sum outputs s'_i, and s'_j, for $j = 1, 2, \ldots, N$ and $i < j$, of an N-bit RCA is given by

$$\begin{aligned}&\text{Cov}(s'_i, s'_j)\\ &= \sum_{k=1}^{i-1}\sum_{l=1}^{j-1}(\rho_{c_{k,\text{var}}, c_{l,\text{var}}}\sigma_{c_{k,\text{var}}}\sigma_{c_{l,\text{var}}}) + \rho_{s_{j,\text{var}}, s_{i,\text{var}}}\sigma_{s_{j,\text{var}}}\sigma_{s_{i,\text{var}}}\\ &\quad + \sum_{k=1}^{i-1}\rho_{c_{k,\text{var}}, s_{j,\text{var}}}\sigma_{c_{k,\text{var}}}\sigma_{s_{j,\text{var}}} + \sum_{l=1}^{j-1}\rho_{c_{l,\text{var}}, s_{i,\text{var}}}\sigma_{c_{l,\text{var}}}\sigma_{s_{i,\text{var}}},\end{aligned} \qquad (54)$$

with $\rho_{k,l}$, the correlation coefficient for cell delays k and l.

Assuming intra-die variations, that is $\rho_{k,l} = 0$ for all RVs k, l with $k \neq l$, $\text{Cov}(s'_i, s'_j)$ is simplified to

$$\text{Cov}(s'_i, s'_j) = (i-1)\sigma^2_{c_{\text{intra}}}. \qquad (55)$$

Assuming inter-die variations, that is $\rho_{k,l} = 1$ for all RVs k, l with $k \neq l$, and the same standard deviation for all RVs, $\sigma_{x_{\text{inter}}}$, $\text{Cov}(s'_i, s'_j)$ is simplified to

$$\text{Cov}(s'_i, s'_j) = ij\sigma^2_{x_{\text{inter}}}. \qquad (56)$$

For a proof, see Appendix B.

Similarly, the following *Lemma* is obtained.

Lemma 2: The covariance between sum output s'_i, and carry output c'_j, for $j = 1, 2, \ldots, N$ and $i < j$, of an N-bit RCA is given by

$$\mathrm{Cov}(s'_i, c'_j) = \sum_{l=1}^{j} \rho_{c_{l,\mathrm{var}}, s_{i,\mathrm{var}}} \sigma_{c_{l,\mathrm{var}}} \sigma_{s_{i,\mathrm{var}}} + \sum_{l=1}^{j} \sum_{k=1}^{i-1} \rho_{c_{l,\mathrm{var}}, c_{k,\mathrm{var}}} \sigma_{c_{l,\mathrm{var}}} \sigma_{c_{k,\mathrm{var}}}. \quad (57)$$

The proof of *Lemma* 2 is similar to the proof of *Lemma* 1, provided in Appendix B.

Covariances can be alternatively obtained using the property $\Sigma_{s'_i} = \mathbf{T}\Sigma_{s_i}\mathbf{T}^T$, where $\Sigma_{s'_i}$ and Σ_{s_i} are the covariance matrices of path delays and primitive cell delays, respectively, connected through a transformation matrix $\mathbf{T}$.

Let RV d_{RCA} describe the maximum delay of an RCA,

$$d_{\mathrm{RCA}} = \max\{\max_{i=1,2,\ldots,N}\{s'_i\}, c'_N\}. \quad (58)$$

In Section IV-D, we exploit Clark's expressions in order to approximate (58). A discussion concerning the respective introduced errors and numerical data is reported in Section VI.

B. Equivalent Derivation of RCA Maximum Delay PDF

Here we demonstrate a joint PDF for the derivation of the PDF of d_{RCA} of (58) that relies on multivariate Gaussian PDF and the covariances presented in Section IV-A. Assuming Gaussian delay variations, the joint PDF of $S'_1, S'_2, \ldots, S'_N, C'_N$ is

$$f_{\mathbf{S}^*}(s'_1, s'_2, \ldots, s'_N, c'_N) = \frac{\exp(-\frac{1}{2}(\mathbf{S}^* - \boldsymbol{\mu})^{\mathbf{T}}\Sigma^{-1}(\mathbf{S}^* - \boldsymbol{\mu}))}{\sqrt{(2\pi)^{N+1}\det(\Sigma)}}, \quad (59)$$

where Σ has elements $\Sigma(k, l)$ with

$$\Sigma(k,l) = \begin{cases} \mathrm{Cov}(S'_k, S'_l), & \text{if } k, l < N+1, \\ \mathrm{Cov}(C'_N, C'_N), & \text{if } k = l = N+1, \\ \mathrm{Cov}(S'_k, C'_N), & \text{otherwise.} \end{cases} \quad (60)$$

is the covariance matrix, $\boldsymbol{\mu} = [\mu_{S'_1}, \mu_{S'_2}, \ldots, \mu_{S'_N}, \mu_{C'_N}]$, $(\mathbf{S}^* - \boldsymbol{\mu})^T$ is the transpose matrix of $(\mathbf{S}^* - \boldsymbol{\mu})$ and $\det(\Sigma)$ is the determinant of Σ. The covariance matrix in (60) is computed by *Lemmas* 1 and 2.

The CDF of d_{RCA} of (58) can be obtained from (59) as the CDF of a multivariate Gaussian distribution, *i.e.*,

$$\mathrm{cdf} = \mathrm{cdf}_{\mathbf{S}^*}(Z, Z, \ldots, Z, Z), \quad (61)$$

which can be efficiently computed [24] and is provided, for example, in MATLAB [25] as function *mvncdf*.

C. Covariances for BSA Outputs in the Presence of Variations

To compute the maximum delay at the output of an N-digit BSA, the maximum delay of ith compressor, $d_{\mathrm{comp}\,i}$, is computed first as

$$d_{\mathrm{comp}\ i} = \max\{r_{1+4i}, r_{2+4i}, r_{3+4i}, r_{4+4i}\}, \quad (62)$$

where r_{j+4i} is the RV expressing the delay of jth path through ith compressor for $j = 1, 2, 3, 4$ and $i = 1, 2, \ldots, N$.

Algorithm 1 Estimation of Maximum Delay PDF Using Clark's Expressions

```
function ESTIMATEPDF(path_mus, path_stds, path_ccs)
    max_mu ← path_mus[1]        ▷ Path mean max. delays
    max_std ← path_stds[1]      ▷ Path max. delay stds
    max_path_ccs ← path_ccs     ▷ Correlation Coeffs
    for id in [2,Npaths] do     ▷ Number of paths
        max_mu, max_std = CLARK (max_mu,
    path_mus[id], max_std, path_stds[id],
    max_path_ccs[id − 1, id])
        for id2 in [id + 2, Npaths] do
            max_path_ccs[id + 1, id2] =
    ESTCC (max_path_ccs[id, id2], path_ccs[id+1, id2])
    return max_mu, max_std
function CLARK(max_mu, path_mus[id],
    max_std, path_stds[id], max_path_ccs[id − 1, id])
    return max_mu, max_std      ▷ Computed by (65)–(70)
function ESTCC(max_path_ccs[id, id2], path_ccs[id+
    1, id2])
    return max_path_ccs         ▷ Computed by (71)
```

Lemma 3: The covariance between r_{1+4i} and r_{2+4i} of an N-digit BSA are given by

$$\mathrm{Cov}(r_{1+4i}, r_{2+4i}) = \rho_{w_{i,\mathrm{var}}, w_{j,\mathrm{var}}} \sigma_{w_{i,\mathrm{var}}} \sigma_{w_{j,\mathrm{var}}} + \rho_{w_{i,\mathrm{var}}, c_{j,\mathrm{var}}} \sigma_{w_{i,\mathrm{var}}} \sigma_{c_{j,\mathrm{var}}} + \rho_{s_{i,\mathrm{var}}, w_{j,\mathrm{var}}} \sigma_{s_{i,\mathrm{var}}} \sigma_{w_{j,\mathrm{var}}} + \rho_{s_{i,\mathrm{var}}, c_{j,\mathrm{var}}} \sigma_{s_{i,\mathrm{var}}} \sigma_{c_{j,\mathrm{var}}}. \quad (63)$$

For a proof, see Appendix C. Covariances between the remainder of the paths are also provided in Appendix C.

RV d_{BSA} that describes the maximum delay of a BSA is

$$d_{\mathrm{BSA}} = \max_{i=1,2,\ldots,N}\{d_{\mathrm{comp}\,i}\}, \quad (64)$$

which is estimated using Algorithm 1.

D. Estimation of RCA and BSA Type-II PDF

After computing the correlation coefficients between the output delays of each adder, the maximum delay, *i.e.*, d_{RCA} or d_{BSA}, is approximated as a Gaussian RV using Clark's expressions [14]. Algorithm 1 evaluates the mean and standard deviation of the maximum of a set of Gaussian RVs in order to estimate the sought PDF. The mean value and standard deviation of maximum delay of output paths p_1 and p_2, with a correlation coefficient ρ_{p_1,p_2}, is approximated as

$$\mu_{\max\{p_1,p_2\}} = v_1, \quad (65)$$

$$\sigma_{\max\{p_1,p_2\}} = \sqrt{v_2 - v_1^2}, \quad (66)$$

$$v_1 = \mu_{p_1}\Phi(\beta) + \mu_{p_2}\Phi(-\beta) + \alpha\phi(\beta), \quad (67)$$

$$v_2 = (\mu_{p_1}^2 + \sigma_{p_1}^2)\Phi(\beta) + (\mu_{p_2}^2 + \sigma_{p_2}^2)\Phi(-\beta) + (\mu_{p_1} + \mu_{p_2})\alpha\phi(\beta), \quad (68)$$

$$\alpha = \sqrt{\sigma_{p_1}^2 + \sigma_{p_2}^2 - 2\rho_{p_1,p_2}\sigma_{p_1}\sigma_{p_2}}, \quad (69)$$

$$\beta = \frac{\mu_{p_1} - \mu_{p_2}}{\alpha}, \quad (70)$$

and $\phi(x)$ is the PDF of standard normal distribution, $\phi(x) = \frac{1}{\sqrt{2\cdot\pi}}\exp(\frac{-x^2}{2})$, and $\Phi(x)$ is the CDF of the same distribution, $\Phi(x) = \int_{-\infty}^{x}\phi(x)dx$ [14]. Eqs. (65)–(70) are conveniently

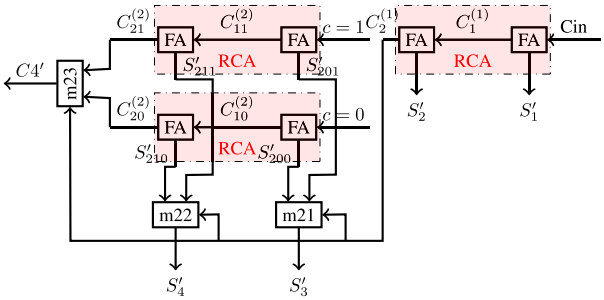

Fig. 3. Example of Carry-Select Adder architecture, with three constituent 2-bit RCAs.

named as function CLARK, called in line 6 of Algorithm 1. Given the correlation coefficients ρ_{p_1,p_3} and ρ_{p_2,p_3}, the correlation coefficient ρ_{p_1,p_2,p_3} is computed as follows

$$\rho_{p_1,p_2,p_3} = \frac{\sigma_1 \rho_{p_1,p_3} \Phi(\beta) + \sigma_2 \rho_{p_2,p_3} \Phi(-\beta)}{\sqrt{v_2 - v_1^2}}. \quad (71)$$

Eq. (71), evaluated by function ESTCC, is called in line 8 of Algorithm 1. After function ESTIMATEPDF finishes its execution, the algorithm returns the estimated mean value and standard deviation of maximum delay.

V. MODEL EXTENSION TO CARRY-SELECT ADDER

The proposed approach is extended to model variations in a Carry-Select Adder (CSL), thus, demonstrating by an example techniques that can be combined with the proposed Type-I model to cover further arithmetic circuits. A CSL with two stages of two bits each is shown in Fig. 3. The maximum delay per output is described as follows

$$S'_1 = S_1 \quad (72)$$

$$S'_2 = S_2 + C_1^{(1)} \quad (73)$$

$$S'_3 = \max\left\{C_2^{(1)} + C_1^{(1)} + m_{21}, S'_{200} + m_{21}, S'_{201} + m_{21}\right\} \quad (74)$$

$$S'_4 = \max\left\{C_2^{(1)} + C_1^{(1)} + m_{22}, S'_{211} + m_{22}, S'_{210} + m_{22}\right\} \quad (75)$$

$$C'_4 = \max\left\{C_2^{(1)} + C_1^{(1)} + m_{23}, C_{21}^{(2)} + C_{11}^{(2)} + m_{23}, C_{20}^{(2)} + C_{10}^{(2)} + m_{23}\right\}, \quad (76)$$

where m_{jk} is the delay of a multiplexer located at jth output of stage k, and $S'_{i,j,k}$ is the delay of the jth output of an RCA located at stage i and receiving a carry-in of constant value k.

The paths that include multiplexers are described by (74)–(76). The key concept in the following approach is to break each of (74)–(76), into three dependent paths, and seek the maximum of the overall resulting set of paths. Specifically, in this way, the maximum delay of the CSL is obtained as the maximum of the paths

$$\begin{aligned} &S'_{10} = S'_1, \quad S'_{20} = S'_2, \\ &S'_{30} = C^{(1)} + m_{21}, \quad S'_{31} = S'_{200} + m_{21}, \\ &S'_{32} = S'_{201} + m_{21}, \quad S'_{40} = C^{(1)} + m_{22}, \\ &S'_{41} = S'_{210} + m_{22}, \quad S'_{42} = S'_{211} + m_{22}, \\ &C'_{40} = C^{(1)} + m_{23}, \quad C'_{41} = C^{(20)} + m_{23}, \\ &C'_{42} = C^{(21)} + m_{23}. \end{aligned} \quad (77)$$

Eq. (77) define a transformation also described as follows

$$\mathbf{D}_{CSL} = \mathbf{T}_{CSL} \cdot \mathbf{D}_{RCA}, \quad (78)$$

where $\mathbf{T}_{CSL}$ denotes the rank-11, 11×12 transformation matrix defined by (77), $\mathbf{D}_{CSL}$ is a 11×1 vector containing path delays in CSL, $\mathbf{D}_{CSL} = [S'_{10}, S'_{20}, S'_{30}, S'_{31}, S'_{32}, S'_{40}, S'_{41}, S'_{42}, C'_{40}, C'_{41}, C'_{42}]$, while $\mathbf{D}_{RCA}$ contains path delays for the constituent RCAs, $\mathbf{D}_{RCA} = [S'_1, S'_2, C^{(1)}, S'_{200}, S'_{210}, C^{(20)}, S'_{201}, S'_{211}, C^{(21)}, m_{21}, m_{22}, m_{23}]$. Eq. (78) reveals that the RVs in $\mathbf{D}_{CSL}$ are jointly gaussian, with a covariance matrix

$$\Sigma_{CSL} = \mathbf{T}_{CSL} \Sigma_{RCA} \mathbf{T}_{CSL}^T. \quad (79)$$

Note that $\mathbf{T}_{CSL}\mathbf{T}_{CSL}^T$ is positive-definite.

Path delays in $\mathbf{D}_{RCA}$ can be expressed as a linear transformation of correlated jointly gaussian RVs. For a 2-bit RCA,

$$\begin{bmatrix} S'_1 \\ S'_2 \\ C'_2 \end{bmatrix} = \begin{bmatrix} \mathbf{I}_2 & \mathbf{A}_2 \\ \mathbf{0}_{1:2} & \mathbf{B}_{1:2} \end{bmatrix} \begin{bmatrix} S_1 \\ S_2 \\ C_1 \\ C_2 \end{bmatrix}. \quad (80)$$

Practically (80) is the model for RCA as described by (8).

For three structurally independent RCAs required for the CSL of Fig. 3, including multiplexer delays, we write

$$\mathbf{D}_{RCA} = \mathbf{T}_{RCA} \mathbf{D}, \quad (81)$$

where

$$\mathbf{T}_{RCA} = \begin{bmatrix} \left(\mathbf{I}_3 \otimes \begin{bmatrix} \mathbf{I}_2 & \mathbf{A}_2 \\ \mathbf{0}_{1:2} & \mathbf{B}_{1:2} \end{bmatrix}\right) & \mathbf{0} \\ \mathbf{0} & \mathbf{I}_3 \end{bmatrix}, \quad (82)$$

$\mathbf{D}$ is a 15×1 vector of jointly gaussian delays of known covariance matrix Σ, and known mean value vector $\boldsymbol{\mu}$, $\mathbf{D} = [S_1, S_2, C_1, C_2, S_{210}, S_{220}, C_{210}, C_{220}, S_{211}, S_{221}, C_{221}, C_{222}, m_{21}, m_{22}, m_{23}]$. Therefore Σ_{RCA} as used in (79) can be derived as

$$\Sigma_{RCA} = \mathbf{T}_{RCA} \Sigma \mathbf{T}_{RCA}^T. \quad (83)$$

By combining (79) and (83), it is obtained that

$$\Sigma_{CSL} = \mathbf{T}_{CSL} \mathbf{T}_{RCA} \Sigma \mathbf{T}_{RCA}^T \mathbf{T}_{CSL}^T. \quad (84)$$

Fig. 4 confirms the agreement of the derived model and M.C. simulations for the cases of 0.1 correlation among primitive cell delays, and 0.3 correlation and 0.3 delay variability.

VI. EXPERIMENTAL RESULTS AND DISCUSSION

This section quantitatively compares Type-I and Type-II PDFs for RCA and BSA maximum delays with a PDF extracted from Monte-Carlo (M.C.) simulations. *Kullback-Leibler Divergence* (KLD) is used as a cost metric for the proposed models. Firstly, the agreement of proposed Type-I models with M.C. simulations is presented for both adders. Secondly, Type-I and Type-II models are compared, examining the two extreme cases for correlation among primitive delays. The comparison includes the cases where inter-die, intra-die or both variations are manifested on the primitive cell delays of an FA. M.C. simulations have been performed using the corresponding circuits graphs, as in SSTA

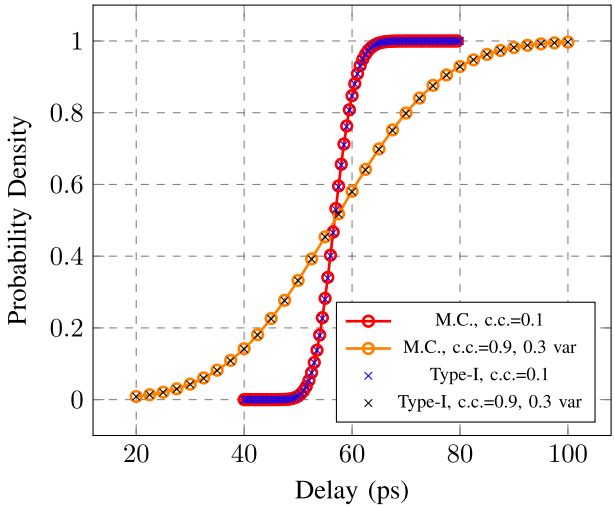

Fig. 4. M.C. and Type-I 4-bit CSL CDFs for certain correlation coefficient (c.c.) between primitive dell delays.

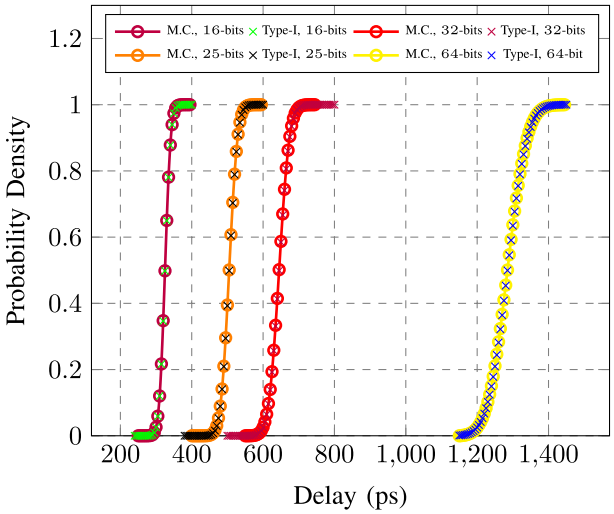

Fig. 6. M.C. and Type-I RCA CDFs for a range of bit-lengths and a correlation coefficient = 0.1 between primitive cell delays.

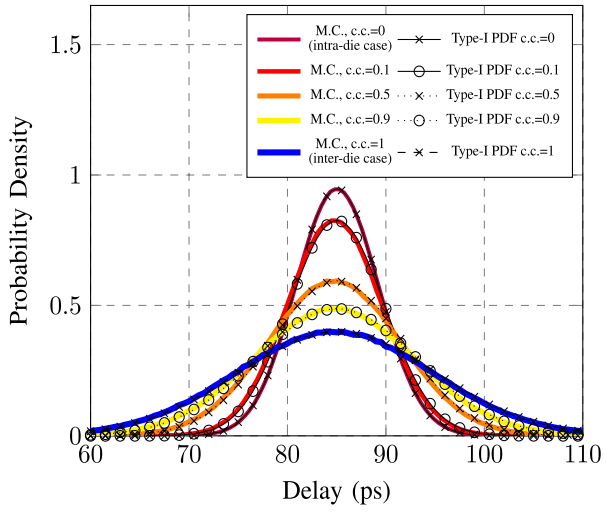

Fig. 5. M.C. and Type-I PDFs of a 4-bit RCA for certain values of correlation coefficient between primitive cell delays.

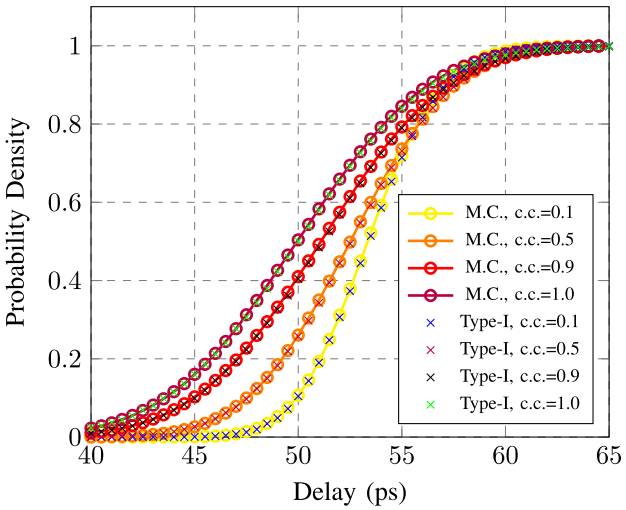

Fig. 7. M.C. and Type-I 4-digit BSA CDFs for certain correlation coefficients between primitive cell delays.

Algorithms [2], [3], [12], and according to modeling assumptions explained in Section III-A. The experimental data reported here are obtained with substantially more extensive simulations than the data presented in [26]. The number of M.C. simulation iterations have been increased from 1500 to $2 \cdot 10^6$. In [3], it is reported that delay variability, *i.e.*, the ratio $\frac{\sigma}{\mu}$, can be as much as 57% according to ITRS. A typical 10% and 20% delay variability has been used for our simulations. Experimental data refer to the case that the underlying variation PDFs of primitive cells are Gaussian.

Fig. 5 presents the PDF of a 4-bit RCA for a range of correlation coefficients and 10% delay variation. Furthermore, Fig. 6 displays the CDFs of RCAs with longer bit-lengths. The respective cases for BSA are shown by Figs. 7 and 8. In all the above cases, Type-I model perfectly agrees with M.C. simulations. It is shown that neither the value of correlation nor the adder bit-width has an negative impact on the accuracy of Type-I models compared to experimental data.

Tables I and II present the mean maximum delay and the standard deviation of maximum delay for the two 4- and 8-bit architectures. Data in all Tables are measured in picoseconds (ps). The value of σ is 10% of the nominal cell delay, while for the case of inter-die variation is 10% of the minimum cell delay. The second columns of Tables I and II demonstrate the values as estimated by M.C. simulations, while the third and fifth columns show the corresponding values as computed by the Type-II and Type-I models, respectively. The columns labeled "Diff." show the difference between the models with respect to the experimental data. Table II demonstrates that BSA achieves smaller standard deviation of maximum delay than RCA. Concerning the Type-II model, we see that the percentage of difference between the mean maximum delay is lower than almost 0.0335%, and its maximum value appears for BSA and both type of variations. In the evaluation of standard deviation of maximum delay, the maximum error is 7.3227% and occurs for BSA and intra-die variations. As indicated by Fig. 13, the mismatch is caused because the exact BSA PDF significantly deviates from a Gaussian distribution. This is also observed for the case that both inter-die and intra-die delay variations are manifested.

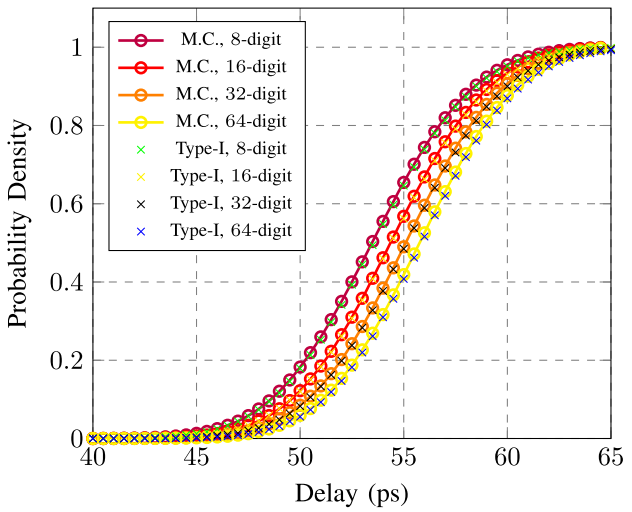

Fig. 8. M.C. and Type-I BSA CDFs for a range of digit lengths and a correlation coefficient = 0.5 between primitive cell delays.

TABLE I
MEAN VALUE OF MAXIMUM DELAY FOR RCA AND BSA

Variation	M.C. (ps)	Type-II (Clark, ps)	Diff. (%)	Type-I (Exact, ps)	Diff. (%)
	4-bit Ripple-Carry Adder				
inter	85.000	85.000	0.0000	85.000	0.0000
intra	85.081	85.081	0.0000	85.081	0.0000
both	85.082	85.081	0.0011	85.081	0.0000
	8-bit Ripple-Carry Adder				
inter	165.000	165.000	0.0000	165.000	0.0000
intra	165.087	165.081	0.0036	165.081	0.0036
both	165.087	165.081	0.0036	165.081	0.0036
	4-digit Borrow-Save Adder				
inter	49.998	50.000	−0.0040	50.000	0.0000
intra	53.675	53.693	−0.0335	53.676	−0.0018
both	53.675	53.693	−0.0335	53.672	0.0055
	8-digit Borrow-Save Adder				
inter	50.000	50.000	0.0000	50.000	0.0000
intra	55.053	55.050	0.0054	55.051	0.0036
both	55.051	55.050	0.0018	55.051	0.0000

On the other hand, the maximum delay distribution of RCA does not significantly differ from a Gaussian distribution, thus, the estimations provided by Clark-based model are very close to that of M.C. simulations. Additionally, Tables I and II reveal that the mean value and standard deviation of the proposed exact Type-I PDFs closely match that of M.C. simulations.

Figs. 12–14 depict PDFs of the maximum propagation delay of 4-bit RCA and BSA as estimated by M.C. simulations. In the same figures, the Type-I and Type-II PDFs are also plotted. It is observed that the Clark-based Type-II model underestimates the standard deviation of maximum delay for BSA (inter-die and) intra-die cases.

In the following, the fitting of the proposed delay models on the experimental data is assessed using the *Kullback-Leibler Divergence*. KLD is assessed between the Type-I and Type-II PDFs, and the obtained values are presented in Table III. A value close to zero for the employed metric indicates a close match between the examined distributions. Examining the fitting between Type-I and Type-II models, it is found that the proposed models for both adders agree to a great extend for the case of inter-die variations, as KLD is in the order of 10^{-15}. Furthermore, for RCA intra-die

TABLE II
STANDARD DEVIATION OF MAXIMUM DELAY FOR RCA AND BSA

Variation	M.C. (ps)	Type-II (Clark, ps)	Diff. (%)	Type-I (Exact, ps)	Diff. (%)
	4-bit Ripple-Carry Adder				
inter	2.000	2.000	0.0000	2.000	0.0000
intra	4.207	4.208	−0.2376	4.208	−0.2376
both	4.658	4.659	−0.2146	4.658	0.0000
	8-bit Ripple-Carry Adder				
inter	4.000	4.000	0.0000	4.000	0.0000
intra	5.812	5.805	0.1204	5.805	0.1204
both	7.057	7.050	0.0991	7.050	0.0991
	4-digit Borrow-Save Adder				
inter	0.998	1.000	−0.2004	1.000	0.0000
intra	2.449	2.333	4.7366	2.448	0.0408
both	2.644	2.539	3.9712	2.641	0.1134
	8-digit Borrow-Save Adder				
inter	1.000	1.000	0.0000	1.000	0.0000
intra	2.144	1.987	7.3227	2.144	0.0000
both	2.367	2.224	6.0414	2.364	0.1267

TABLE III
KULLBACK-LEIBLER DIVERGENCE

Variation	KLD(Type-I‖Type-II)		KLD(M.C.‖Type-II)	
	RCA	BSA	RCA	BSA
inter-die	1.3124E−15	1.7500E−16	-	-
intra-die	2.0211E−04	0.0125	3.2767E−04	0.0130
both	1.3469E−04	0.0072	2.7824E−04	0.0079

or both inter-die and intra-die cases, the fitting between Type-I and Type-II models is satisfactory as KLD is in the order of 10^{-4}. The same is observed for the Type-II model and experimental PDF. This means that the exact PDFs for RCA closely resemble a Gaussian distribution for all types of variations. As expected, the worst fitting occurs for the case of BSA Type-II model under only intra-die or both inter-die and intra-die delay variations, with a KLD value of 0.0125 and 0.0072, respectively. The reason of this mismatch is investigated by the following test: we construct Gaussian PDFs with the mean value and standard deviation obtained using the Type-I model, and subsequently compute the KLD between the constructed PDF and the Type-I model, which is not Gaussian. It is found that the KLD is 0.0102 and 0.0058 for intra-die, and both inter-die and intra-die BSA cases, respectively. The previous test confirms that, although the KLD is incrementally improved w.r.t. KLD(Type-I‖Type-II) case, the shape of distribution, and neither the mean value nor the standard deviation, is responsible for the mismatch between the Type-I and Type-II BSA models. The same conclusions follow from KLD(M.C.‖Type-II), as values closely match.

Additionally, Figs. 9 and 10 present the mean delay value and standard deviation of maximum delay for a range of BSA word lengths and 10% and 20% delay variations, respectively. Data refer to only intra-die variation, which is the case with the larger error between the Type-I and Type-II models. The error is greater for the maximum-delay standard deviation, while the mean value, as estimated by the two models, shows an (absolute) error which is smaller than 0.23%. In more detail, Clark expressions either underestimate or overestimate the mean value of maximum delay, but they always underestimate the respective standard deviation. For example, Clark-based Type-II model underestimates the standard deviation of maximum delay of 256-digit BSA as much as 16%. Concerning the

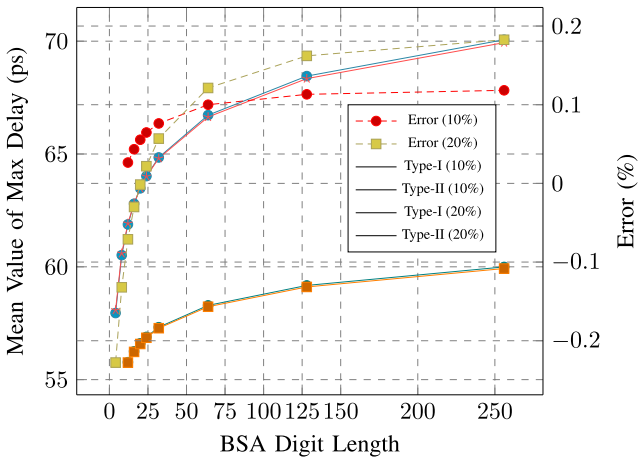

Fig. 9. Mean Value of Maximum Delay for N-digit BSA.

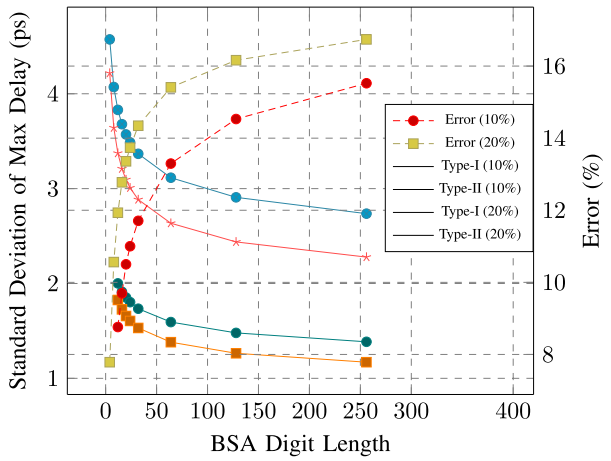

Fig. 10. Standard Deviation of Maximum Delay for N-digit BSA.

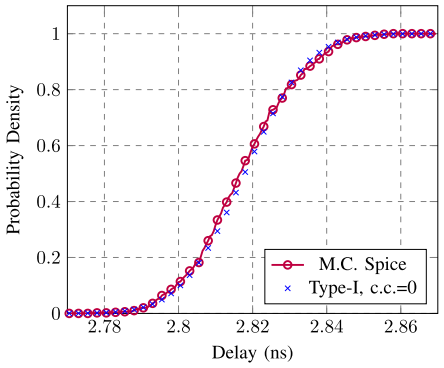

Fig. 11. M.C. Spice and Type-I CDF for a 4-bit RCA in the presence of intra-die channel length variations.

extension of the discussed delay models to longer adder word lengths, we see that the Clark-based Type-II models can be easily extended to longer word-length structures, however, introducing errors due to their simplifying Gaussian assumption for the maximum delay PDF. On the other hand, the exact Type-I models can be cumbersome due to the large number of required integrations. Nevertheless, the complexity of the proposed models can be reduced if we choose to investigate the delay characteristics only for a subset of paths most likely to be critical, chosen under nominal conditions. This technique is widely adopted in M.C. simulations [3].

TABLE IV
TYPE-I $\mu + 3\sigma$ WORST-CASE DELAY FOR 8-BIT RCA AND BSA

Variation	Ripple-Carry Adder (ps)	Borrow-Save Adder (ps)
inter-die	170.000	53.000
intra-die	182.496	61.483
both	186.231	62.143

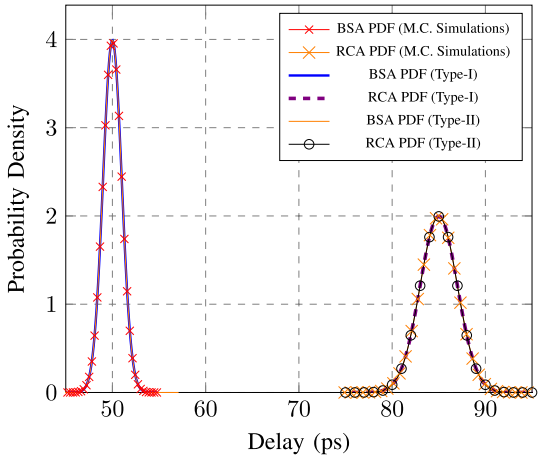

Fig. 12. PDFs of maximum propagation delay for a 4-bit RCA and BSA, estimated by M.C. simulations, Type-I and Type-II models, when only inter-die variations are manifested.

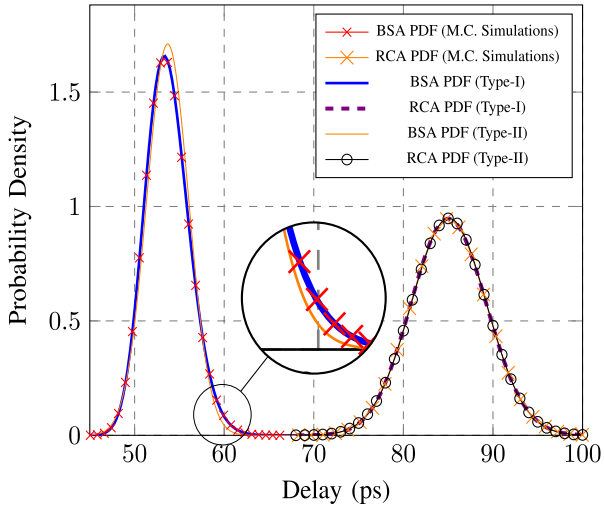

Fig. 13. PDFs of maximum propagation delay for a 4-bit RCA and BSA, estimated by M.C. simulations, Type-I and Type-II models, when only intra-die variations are manifested.

The proposed Type-I models have been also compared with experimental obtained from M.C. Spice simulations. The employed Spice models refer to BSIM-4 MOSFET models and a low-power 45-nm technology. CPL FAs have been used as primitive cells. The maximum delay of RCA has been measured when the critical path delay under nominal circumstances is sensitized and intra-die channel length variations take place. Fig. 11 shows the CDF of M.C. Spice simulations and a Type-I RCA CDF. For the Type-I model, a multivariate Gaussian PDF has been used for the PDF of sum and carry cell delays. The employed PDF uses the cell delay mean values and variances obtained from M.C. simulations. In this case, it is assumed that there is no correlation between

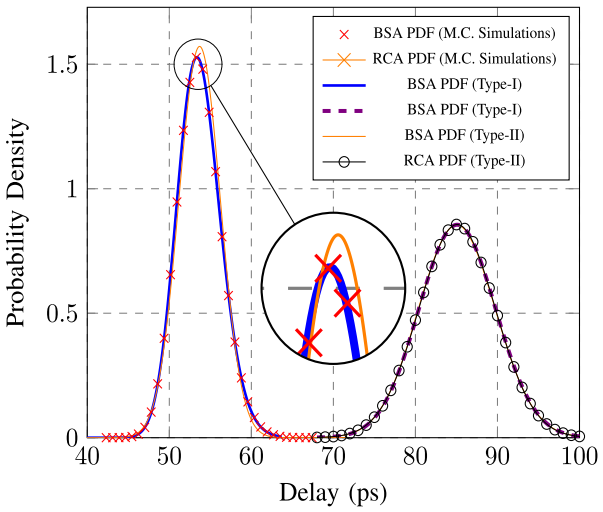

Fig. 14. PDFs of maximum propagation delay for a 4-bit RCA and BSA, estimated by M.C. simulations, Type-I and Type-II models, when both inter-die and intra-die variations are manifested.

primitive delays of Type-I model. Fig. 11 reveals that the proposed Type-I model agrees with data obtained with M.C. measurements.

Summarizing, it is inferred from Table IV that BSA achieves smaller worst-case maximum delay, *i.e.*, $\mu + 3\sigma$, than RCA. From a variation-tolerance perspective, this timing margin is favorable, as BSA can tolerate increased delay variability w.r.t. that of RCA. Furthermore, Fig. 9 shows that, as the word length of BSA increases, the worst-case delay under variability conditions increases only slightly, as its mean maximum delay, in contrast with RCA, whose worst-case delay increases at least linearly to its word length.

VII. Conclusion

We present two statistical delay models for the Maximum Delay PDFs of RCA and BSA. The proposed models can capture every correlation value between FA delay variations, and characterize the delay of adders from a static perspective. The Type-I model describes the Maximum Delay of RCA and BSA with exact PDFs, while the Type-II model relies on Clark's expressions and approximates the exact PDFs with Gaussian PDFs. It is found that both models are in agreement with experimental data obtained by M.C. simulations as the *Kullback-Leibler Divergence* metric indicates, but not with the same accuracy. While the Type-II Clark-based model introduces unavoidable errors in the estimation of mean value and standard deviation of maximum delay, which can be attributed to the Gaussian assumption of the model, it is found to be simpler than the proposed Type-I exact PDFs. However, the latter provide an extract derivation of mean maximum delay and standard deviation for RCA and BSA.

Appendix A
Derivation of Inverse Transformation Matrix

We seek the inverse of the transformation matrix

$$\mathbf{T}_{2N} = \begin{bmatrix} \mathbf{I}_N & \mathbf{A}_N \\ \mathbf{0}_N & \mathbf{B}_N \end{bmatrix}. \tag{85}$$

where $\mathbf{A}_N$ and $\mathbf{B}_N$ are defined in Section III-B.

Proof: It is sufficient to show that if

$$\mathbf{T}_{2N} \cdot \mathbf{H}_{2N} = \mathbf{I}_{2N} \quad \text{and } \mathbf{H}_{2N} \cdot \mathbf{T}_{2N} = \mathbf{I}_{2N}, \tag{86}$$

where $\mathbf{C}_N$ and $\mathbf{D}_N$ are defined in Section III-B, then it holds that $\mathbf{H_{2N}} = \mathbf{T_{2N}^{-1}}$.

$$\mathbf{T}_{2N} \cdot \mathbf{H}_{2N} = \begin{bmatrix} \mathbf{I}_N & \mathbf{A}_N \\ \mathbf{0}_N & \mathbf{B}_N \end{bmatrix} \cdot \begin{bmatrix} \mathbf{I}_N & \mathbf{C}_N \\ \mathbf{0}_N & \mathbf{D}_N \end{bmatrix} \tag{87}$$

$$= \begin{bmatrix} \mathbf{I}_N & \mathbf{I}_N \cdot \mathbf{C}_N + \mathbf{A_N} \cdot \mathbf{D_N} \\ \mathbf{0}_N & \mathbf{B}_N \cdot \mathbf{D}_N \end{bmatrix} \tag{88}$$

Let $\mathbf{L}_N = \mathbf{B}_N \cdot \mathbf{D}_N$, and l_{ij} be the element of matrix $\mathbf{L}_N$ in ith row and jth column. For the first row ($i = 1$) it holds that

$$l_{11} = \sum_{k=1}^{N} b_{1k} d_{k1} = b_{11} d_{11} + \sum_{k=2}^{N} b_{1k} 0 = 1, \tag{89}$$

$$l_{1j} = \sum_{k=1}^{N} b_{1k} d_{kj} = b_{11} d_{1j} + \sum_{k=2}^{N} b_{1k} d_{kj} \tag{90}$$

$$= b_{11} d_{1j} + b_{ij} d_{jj} = -1 \cdot 1 + 1 \cdot 1 = 0. \tag{91}$$

Furthermore, for $i \neq 1$

$$l_{ij} = \sum_{k=1}^{N} b_{ik} d_{kj} = b_{ii} d_{ij} = \begin{cases} b_{ii} d_{ii} = 1 & \text{if } i = j, i \neq 1 \\ b_{ii} d_{ij} = 0 & \text{if } i \neq j, i \neq 1. \end{cases} \tag{92}$$

Thus, $\mathbf{L}_N$ is an identity matrix. Also let $\mathbf{M}_N = \mathbf{A}_N \cdot \mathbf{D}_N$.

For the first row ($i = 1$)

$$m_{1j} = \sum_{k=1}^{N} a_{1k} d_{kj} = \sum_{k=1}^{N} 0 d_{kj} = 0, \tag{93}$$

while for the first column ($j = 1, i \neq 1$)

$$m_{i1} = \sum_{k=1}^{N} a_{ik} d_{k1} = a_{i1} d_{11} = 1. \tag{94}$$

Additionally, for $i \neq 1$ and $j \neq 1$

$$m_{ij} = \sum_{k=1}^{N} a_{ik} d_{kj} = \sum_{k=1}^{i-1} a_{ik} d_{kj} + \sum_{k=i}^{N} a_{ik} d_{kj} \tag{95}$$

$$= \sum_{k=1}^{i-1} 1 \cdot d_{kj} + \sum_{k=i}^{N} 0 \cdot d_{kj} = \sum_{k=1}^{i-1} d_{kj} \tag{96}$$

$$= d_{1j} + \sum_{k=2}^{i-1} d_{kj} = -1 + \sum_{k=2}^{i-1} d_{kj} \tag{97}$$

$$= \begin{cases} -1 + d_{jj} = -1 + 1 = 0 & \text{if } j < i, i, j \neq 1 \\ -1 + \sum_{k=2}^{i-1} 0 = -1 + 0 = -1 & \text{if } j \geq i, i, j \neq 1. \end{cases} \tag{98}$$

Due to (93)–(98), $\mathbf{M}_N = \mathbf{A}_N \cdot \mathbf{D}_N = -\mathbf{C}_N$. Hence

$$\mathbf{T_{2N}} \cdot \mathbf{H_{2N}} = \begin{bmatrix} \mathbf{I}_N & \mathbf{I}_N \cdot \mathbf{C}_N + \mathbf{A}_N \cdot \mathbf{D}_N \\ \mathbf{0}_N & \mathbf{B}_N \cdot \mathbf{D}_N \end{bmatrix} \tag{99}$$

$$= \begin{bmatrix} \mathbf{I}_N & \mathbf{C}_N - \mathbf{C}_N \\ \mathbf{0}_N & \mathbf{I}_N \end{bmatrix} = \mathbf{I}_{2N}. \tag{100}$$

It can also be proven that $\mathbf{H}_{2N} \cdot \mathbf{T}_{2N} = \mathbf{I}_{2N}$. ■

APPENDIX B
PROOF OF LEMMA 1

Proof: For the case of RCA and using (1)

$$E[s'_i \cdot s'_j] = E[(s_{i',\text{nom}} + s_{i',\text{var}})(s_{j',\text{nom}} + s_{j',\text{var}})] \quad (101)$$

$$= E[s_{i',\text{nom}}s_{j',\text{nom}} + s_{i',\text{nom}}s_{j',\text{var}} + s_{i',\text{var}}s_{j',\text{nom}} + s_{i',\text{var}}s_{j',\text{var}}] \quad (102)$$

$$= \mu_{s_{i',\text{nom}}}\mu_{s_{j',\text{nom}}} + E[s_{i',\text{var}}s_{j',\text{var}}], \quad (103)$$

as pairs $s_{i',\text{nom}}, s_{j',\text{var}}$ and $s_{j',\text{nom}}, s_{i',\text{var}}$ are independent and $E[s_{i',\text{var}}] = E[s_{j',\text{var}}] = 0$.

Using the property $E[kl] = \rho_{k,l}\sigma_k\sigma_l + \mu_k\mu_l$ for any two RVs k, l, it follows that

$$\begin{aligned} &E[s_{i',\text{var}} \cdot s_{j',\text{var}}] \\ &= E[(\sum_{k=1}^{i-1} c_{k,\text{var}} + s_{i,\text{var}})(\sum_{l=1}^{l-1} c_{l,\text{var}} + s_{j,\text{var}})] \\ &= E[\sum_{k=1}^{i-1} c_{k,\text{var}} \sum_{l=1}^{j-1} c_{l,\text{var}}] + E[\sum_{k=1}^{i-1} c_{k,\text{var}}s_{j,\text{var}}] \\ &\quad + E[\sum_{l=1}^{j-1} c_{l,\text{var}}s_{i,\text{var}}] + E[s_{i,\text{var}}s_{j,\text{var}}] \quad (104) \\ &= \sum_{k=1}^{i-1}\sum_{l=1}^{j-1}(\rho_{c_{k,\text{var}},c_{l,\text{var}}}\sigma_{c_{k,\text{var}}}\sigma_{c_{l,\text{var}}}) + \rho_{s_{j,\text{var}},s_{i,\text{var}}}\sigma_{s_{j,\text{var}}}\sigma_{s_{i,\text{var}}} \\ &\quad + \sum_{k=1}^{i-1}\rho_{c_{k,\text{var}},s_{j,\text{var}}}\sigma_{c_{k,\text{var}}}\sigma_{s_{j,\text{var}}} + \sum_{l=1}^{j-1}\rho_{c_{l,\text{var}},s_{i,\text{var}}}\sigma_{c_{l,\text{var}}}\sigma_{s_{i,\text{var}}}. \quad (105) \end{aligned}$$

Furthermore,

$$\begin{aligned} &E[s_{i'}]E[s_{j'}] \\ &= E[s_{i',\text{nom}} + s_{i',\text{var}}]E[s_{j',\text{nom}} + s_{j',\text{var}}] \quad (106) \\ &= (E[s_{i',\text{nom}}] + E[s_{i',\text{var}}])(E[s_{j',\text{nom}}] + E[s_{j',\text{var}}]) \quad (107) \\ &= \mu_{s_{i',\text{nom}}}\mu_{s_{j',\text{nom}}}. \quad (108) \end{aligned}$$

Thus, combining (103), (105) and (108) it follows that

$$\begin{aligned} &\text{Cov}(s'_i, s'_j) \\ &= \sum_{k=1}^{i-1}\sum_{l=1}^{j-1}(\rho_{c_{k,\text{var}},c_{l,\text{var}}}\sigma_{c_{k,\text{var}}}\sigma_{c_{l,\text{var}}}) + \rho_{s_{j,\text{var}},s_{i,\text{var}}}\sigma_{s_{j,\text{var}}}\sigma_{s_{i,\text{var}}} \\ &\quad + \sum_{k=1}^{i-1}\rho_{c_{k,\text{var}},s_{j,\text{var}}}\sigma_{c_{k,\text{var}}}\sigma_{s_{j,\text{var}}} + \sum_{l=1}^{j-1}\rho_{c_{l,\text{var}},s_{i,\text{var}}}\sigma_{c_{l,\text{var}}}\sigma_{s_{i,\text{var}}}. \quad (109) \end{aligned}$$

■

APPENDIX C
PROOF OF LEMMA 3

Proof: For the computation of $\text{Cov}(r_{1+4i}, r_{2+4i})$

$$\text{Cov}(r_{1+4i}, r_{2+4i}) = E[r_{1+4i} \cdot r_{2+4i}] - E[r_{1+4i}] \cdot E[r_{2+4i}], \quad (110)$$

we have that

$$\begin{aligned} E[r_{1+4i} \cdot r_{2+4i}] &= E[(w_i + s_i)(w_j + c_j)] \quad (111) \\ &= E[(w_{i,\text{nom}} + w_{i,\text{var}})(w_{j,\text{nom}} + w_{j,\text{var}})] \\ &\quad + E[(w_{i,\text{nom}} + w_{i,\text{var}})(c_{j,\text{nom}} + c_{j,\text{var}})] \\ &\quad + E[(s_{i,\text{nom}} + s_{i,\text{var}})(s_{j,\text{nom}} + s_{j,\text{var}})] \\ &\quad + E[(w_{i,\text{nom}} + w_{i,\text{var}})(c_{j,\text{nom}} + c_{j,\text{var}})] \quad (112) \\ &= \mu_w^2 + E[w_{i,\text{var}}w_{j,\text{var}}] + \mu_w\mu_c \\ &\quad + E[w_{i,\text{var}}c_{j,\text{var}}] + \mu_s^2 + E[s_{i,\text{var}}s_{j,\text{var}}] \\ &\quad + \mu_w\mu_c + E[w_{i,\text{var}}c_{j,\text{var}}]. \quad (113) \\ E[r_{1+4i}r_{2+4i}] &= E[(w_i + s_i)]E[(w_j + c_j)] \quad (114) \\ &= (E[w_i] + E[s_i])(E[w_j] + E[c_j]) \quad (115) \\ &= \mu_w^2 + \mu_w\mu_c + \mu_s\mu_w + \mu_s\mu_c. \quad (116) \end{aligned}$$

Combining (110)–(116), it follows that

$$\begin{aligned} &\text{Cov}(r_{1+4i}, r_{2+4i}) \\ &= -\mu_w^2 - \mu_w\mu_c - \mu_s^2 - \mu_w\mu_c \\ &\quad + \mu_w^2 + E[w_{i,\text{var}}w_{j,\text{var}}] + \mu_w\mu_c + E[w_{i,\text{var}}c_{j,\text{var}}] \\ &\quad + \mu_s^2 + E[s_{i,\text{var}}s_{j,\text{var}}] + \mu_w\mu_c + E[w_{i,\text{var}}c_{j,\text{var}}] \quad (117) \\ &= E[w_{i,\text{var}}w_{j,\text{var}}] + E[w_{i,\text{var}}c_{j,\text{var}}] \\ &\quad + E[s_{i,\text{var}}s_{j,\text{var}}] + E[w_{i,\text{var}}c_{j,\text{var}}] \quad (118) \\ &= \rho_{w_{i,\text{var}},w_{j,\text{var}}}\sigma_{w_{i,\text{var}}}\sigma_{w_{j,\text{var}}} + \rho_{w_{i,\text{var}},c_{j,\text{var}}}\sigma_{w_{i,\text{var}}}\sigma_{c_{j,\text{var}}} \\ &\quad + \rho_{s_{i,\text{var}},w_{j,\text{var}}}\sigma_{s_{i,\text{var}}}\sigma_{w_{j,\text{var}}} + \rho_{s_{i,\text{var}},c_{j,\text{var}}}\sigma_{s_{i,\text{var}}}\sigma_{c_{j,\text{var}}}. \quad (119) \end{aligned}$$

Similarly, it is proved that

$$\begin{aligned} &\text{Cov}(r_{1+4i}, r_{3+4j}) \\ &= \rho_{w_{i,\text{var}},t_{j-1,\text{var}}}\sigma_{w_{i,\text{var}}}\sigma_{t_{j-1,\text{var}}} + \rho_{w_{i,\text{var}},s_{j,\text{var}}}\sigma_{w_{i,\text{var}}}\sigma_{s_{j,\text{var}}} \\ &\quad + \rho_{s_{i,\text{var}},t_{j-1,\text{var}}}\sigma_{s_{i,\text{var}}}\sigma_{t_{j-1,\text{var}}} + \rho_{s_{i,\text{var}},s_{j,\text{var}}}\sigma_{s_{i,\text{var}}}\sigma_{s_{j,\text{var}}}, \quad (120) \end{aligned}$$

$$\begin{aligned} &\text{Cov}(r_{1+4i}, r_{4+4j}) \\ &= \rho_{w_{i,\text{var}},t_{j-1,\text{var}}}\sigma_{w_{i,\text{var}}}\sigma_{t_{j-1,\text{var}}} + \rho_{w_{i,\text{var}},c_{j,\text{var}}}\sigma_{w_{i,\text{var}}}\sigma_{c_{j,\text{var}}} \\ &\quad + \rho_{s_{i,\text{var}},t_{j-1,\text{var}}}\sigma_{s_{i,\text{var}}}\sigma_{t_{j-1,\text{var}}} + \rho_{s_{i,\text{var}},c_{j,\text{var}}}\sigma_{s_{i,\text{var}}}\sigma_{c_{j,\text{var}}}, \quad (121) \end{aligned}$$

$$\begin{aligned} &\text{Cov}(r_{1+4i}, r_{1+4j}) \\ &= \rho_{w_{i,\text{var}},w_{j,\text{var}}}\sigma_{w_{i,\text{var}}}\sigma_{w_{j,\text{var}}} + \rho_{w_{i,\text{var}},s_{j,\text{var}}}\sigma_{w_{i,\text{var}}}\sigma_{s_{j,\text{var}}} \\ &\quad + \rho_{s_{i,\text{var}},w_{j,\text{var}}}\sigma_{s_{i,\text{var}}}\sigma_{w_{j,\text{var}}} + \rho_{s_{i,\text{var}},s_{j,\text{var}}}\sigma_{s_{i,\text{var}}}\sigma_{s_{j,\text{var}}}, \quad (122) \end{aligned}$$

$$\begin{aligned} &\text{Cov}(r_{2+4i}, r_{3+4j}) \\ &= \rho_{w_{i,\text{var}},t_{j-1,\text{var}}}\sigma_{w_{i,\text{var}}}\sigma_{t_{j-1,\text{var}}} + \rho_{w_{i,\text{var}},s_{j,\text{var}}}\sigma_{w_{i,\text{var}}}\sigma_{s_{j,\text{var}}} \\ &\quad + \rho_{c_{i,\text{var}},t_{j-1,\text{var}}}\sigma_{c_{i,\text{var}}}\sigma_{t_{j-1,\text{var}}} + \rho_{c_{i,\text{var}},s_{j,\text{var}}}\sigma_{c_{i,\text{var}}}\sigma_{s_{j,\text{var}}}, \quad (123) \end{aligned}$$

$$\begin{aligned} &\text{Cov}(r_{3+4i}, r_{4+4j}) \\ &= \rho_{t_{i-1,\text{var}},t_{j-1,\text{var}}}\sigma_{t_{i-1,\text{var}}}\sigma_{t_{j-1,\text{var}}} \\ &\quad + \rho_{t_{i-1,\text{var}},c_{j,\text{var}}}\sigma_{t_{i-1,\text{var}}}\sigma_{c_{j,\text{var}}} + \rho_{s_{i,\text{var}},t_{j-1,\text{var}}}\sigma_{s_{i,\text{var}}}\sigma_{t_{j-1,\text{var}}} \\ &\quad + \rho_{s_{i,\text{var}},c_{j,\text{var}}}\sigma_{s_{i,\text{var}}}\sigma_{c_{j,\text{var}}}, \quad (124) \end{aligned}$$

$$\begin{aligned}\mathrm{Cov}(r_{2+4i}, r_{2+4j}) &= \rho_{w_{i,\mathrm{var}},w_{j,\mathrm{var}}}\sigma_{w_{i,\mathrm{var}}}\sigma_{w_{j,\mathrm{var}}} + \rho_{w_{i,\mathrm{var}},c_{j,\mathrm{var}}}\sigma_{w_{i,\mathrm{var}}}\sigma_{c_{j,\mathrm{var}}} \\ &\quad + \rho_{c_{i,\mathrm{var}},w_{j,\mathrm{var}}}\sigma_{c_{i,\mathrm{var}}}\sigma_{w_{j,\mathrm{var}}} + \rho_{c_{i,\mathrm{var}},c_{j,\mathrm{var}}}\sigma_{c_{i,\mathrm{var}}}\sigma_{c_{j,\mathrm{var}}}, \end{aligned} \tag{125}$$

$$\begin{aligned}\mathrm{Cov}(r_{3+4i}, r_{3+4i}) &= \rho_{t_{i-1,\mathrm{var}},t_{j-1,\mathrm{var}}}\sigma_{t_{i-1,\mathrm{var}}}\sigma_{t_{j-1,\mathrm{var}}} \\ &\quad + \rho_{t_{i-1,\mathrm{var}},s_{j,\mathrm{var}}}\sigma_{t_{i-1,\mathrm{var}}}\sigma_{s_{j,\mathrm{var}}} + \rho_{s_{i,\mathrm{var}},t_{j-1,\mathrm{var}}}\sigma_{s_{i,\mathrm{var}}}\sigma_{t_{j-1,\mathrm{var}}} \\ &\quad + \rho_{s_{i,\mathrm{var}},s_{j,\mathrm{var}}}\sigma_{s_{i,\mathrm{var}}}\sigma_{s_{j,\mathrm{var}}}, \end{aligned} \tag{126}$$

$$\begin{aligned}\mathrm{Cov}(r_{4+4i}, r_{4+4j}) &= \rho_{t_{i-1,\mathrm{var}},t_{j-1,\mathrm{var}}}\sigma_{t_{i-1,\mathrm{var}}}\sigma_{t_{j-1,\mathrm{var}}} \\ &\quad + \rho_{t_{i-1,\mathrm{var}},c_{j,\mathrm{var}}}\sigma_{t_{i-1,\mathrm{var}}}\sigma_{c_{j,\mathrm{var}}} + \rho_{c_{i,\mathrm{var}},t_{j-1,\mathrm{var}}}\sigma_{c_{i,\mathrm{var}}}\sigma_{t_{j-1,\mathrm{var}}} \\ &\quad + \rho_{c_{i,\mathrm{var}},c_{j,\mathrm{var}}}\sigma_{c_{i,\mathrm{var}}}\sigma_{c_{j,\mathrm{var}}}. \end{aligned} \tag{127}$$

■

REFERENCES

[1] R. Garg, *Anal. Design of Resilient VLSI Circuits: Mitigating Soft Errors and Process Variations*. New York, NY, USA: Springer, 2009.

[2] A. Srivastava, D. Sylvester, and D. Blaauw, *Statistical Analysis and Optimization for VLSI: Timing and Power*. New York, NY, USA: Springer, 2006.

[3] D. Boning, M. Orshansky, and S. Nassif, *Design for Manufacturability and Statistical Design: A Constructive Approach*. New York, NY, USA: Springer, 2007.

[4] K. J. Kuhn, "Reducing variation in advanced logic technologies: Approaches to process and design for manufacturability of nanoscale CMOS," in *Proc. IEDM Tech. Dig.*, Dec. 2007, pp. 471–474.

[5] M. Eisele, J. Berthold, D. Schmitt-Landsiedel, and R. Mahnkopf, "The impact of intra-die device parameter variations on path delays and on the design for yield of low voltage digital circuits," *IEEE Trans. Very Large Scale Integr. (VLSI) Syst.*, vol. 5, no. 4, pp. 360–368, Dec. 1997.

[6] E. Baravelli, M. Jurczak, N. Speciale, K. D. Meyer, and A. Dixit, "Impact of LER and random dopant fluctuations on FinFET matching performance," *IEEE Trans. Nanotechnol.*, vol. 7, no. 3, pp. 291–298, May 2008.

[7] C. Visweswariah *et al.*, "First-order incremental block-based statistical timing analysis," *IEEE Trans. Comput.-Aided Des. Integr. Circuits Syst.*, vol. 25, no. 10, pp. 2170–2180, Oct. 2006.

[8] K. Papachatzopoulos, I. Kouretas, and V. Paliouras, "Dynamic delay variation behaviour of rns multiply-add architectures," in *Proc. IEEE Int. Symp. Circuits Syst. (ISCAS)*. May 2016, pp. 1978–1981.

[9] K. Papachatzopoulos and V. Paliouras, "Low-power addition with borrow-save adders under threshold voltage variability," *IEEE Trans. Circuits Syst. II, Exp. Briefs*, vol. 65, no. 5, pp. 572–576, 2018.

[10] K. Bernstein *et al.*, "High-performance CMOS variability in the 65-nm regime and beyond," *IBM J. Res. Develop.*, vol. 50, nos. 4–5, pp. 433–449, Jul. 2006.

[11] M. Alioto and G. Palumbo, "Impact of supply voltage variations on full adder delay: Analysis and comparison," *IEEE Trans. Very Large Scale Integr. (VLSI) Syst.*, vol. 14, no. 12, pp. 1322–1335, Dec. 2006.

[12] M. Alioto, G. Scotti, A. Trifiletti, "A novel framework to estimate the path delay variability on the back of an envelope via the fan-out-of-4 metric," *IEEE Trans. Circuits Syst. I, Reg. Papers*, vol. 64, no. 8, pp. 2073–2085, Aug. 2017.

[13] M. H. Abu-Rahma and M. Anis, "A statistical design-oriented delay variation model accounting for within-die variations," *IEEE Trans. Comput.-Aided Des. Integr. Circuits Syst.*, vol. 27, no. 11, pp. 1983–1995, Nov. 2008.

[14] C. E. Clark, "The greatest of a finite set of random variables," *Operations Res.*, vol. 9, no. 2, pp. 145–162, 1961.

[15] N. H. Weste and D. Harris, *CMOS VLSI Design: A Circuits and Systems Perspective*. Noida, India: Pearson, 2015.

[16] B. Parhami, *Comput. Arithmetic: Algorithms and Hardware Designs*. New York, NY, USA: Oxford Univ. Press, 2009.

[17] P. Kornerup, "Reviewing high-radix signed-digit adders," *IEEE Trans. Comput.*, vol. 64, no. 5, pp. 1502–1505, May 2015.

[18] P. Kornerup, "Reviewing 4-to-2 adders for multi-operand addition," in *Proc. IEEE Int. Conf. Appl.-Specific Syst., Architectures, Processors*, Jul. 2005, pp. 218–229.

[19] S. Abolmaali, N. Mansouri-Ghiasi, M. Kamal, A. Afzali-Kusha, and M. Pedram, "Efficient critical path identification based on viability analysis method considering process variations," *IEEE Trans. Very Large Scale Integr. (VLSI) Syst.*, vol. 25, no. 9, pp. 2668–2672, Sep. 2017.

[20] M. Alioto and G. Palumbo, "Analysis and comparison on full adder block in submicron technology," *IEEE Trans. Very Large Scale Integr. (VLSI) Syst.*, vol. 10, no. 6, pp. 806–823, Dec. 2002.

[21] M. Alioto, and G. Palumbo, "Very fast carry energy efficient computation based on mixed dynamic/transmission-gate full adders," *Electron. Lett.*, vol. 43, no. 13, pp. 707–709, Jun. 2007.

[22] H. Naseri and S. Timarchi, "Low-power and fast full adder by exploring new XOR and XNOR gates," *IEEE Trans. Very Large Scale Integr. (VLSI) Syst.*, vol. 26, no. 8, pp. 1481–1493, Aug. 2018.

[23] A. Papoulis and S. U. Pillai, *Probability, Random Variables, and Stochastic Processes*. New York, NY, USA: Tata McGraw-Hill, 2002.

[24] A. Genz and F. Bretz, "Numerical computation of multivariate t-probabilities with application to power calculation of multiple contrasts," *J. Statist. Comput. Simul.*, vol. 63, no. 4, pp. 103–117, 1999.

[25] *Multivariate Normal Cumulative Distribution Function*. Accessed: Sep. 24, 2018. [Online]. Available: https://www.mathworks.com/help/stats/mvncdf.html

[26] K. Papachatzopoulos and V. Paliouras, "Reduction of delay variations in arithmetic circuits using a redundant representation," in *Proc. 5th Int. Conf. Mod. Circuits Syst. Technol. (MOCAST)*. May 2016, pp. 1–4.

Kleanthis Papachatzopoulos (S'16) received the Diploma degree in electrical and computer engineering and the M.Sc. degree in integrated hardware-software systems from the University of Patras, Patras, Greece, in 2016 and 2018, respectively.

He is currently a Research Assistant with the VLSI Design Laboratory, Electrical and Computer Engineering Department, University of Patras. His current research interests include very large-scale integration architectures for signal processing and computer arithmetic.

Vassilis Paliouras (S'90–M'95) is currently an Associate Professor with the Electrical and Computer Engineering Department, University of Patras, Patras, Greece. He has authored or co-authored two books and more than 130 research articles in international journals, conferences, and book chapters. He has edited four books. His current research interests include very large-scale integration architectures for signal processing and communications, low-power digital design, and computer arithmetic.

Mr. Paliouras was a recipient of the IEEE CASS Guillemin-Cauer Best-Paper Award for the year 2000. He has served as a General Co-Chair for the International Workshop on Power and Timing Modeling, Optimization and Simulation (PATMOS 2004), the Technical Program Chair for PATMOS 2005 and the IEEE Workshop on Signal Processing Systems Implementation 2005, a Technical Program Co-Chair for the IEEE International Conference on Electronics Circuits and Systems 2010, and a European Liaison for the IEEE ISCAS 2012, South Korea. He has served on editorial boards for journals and technical program committees of numerous conferences in the areas of circuits, systems, signal processing, and communications.